BAND MODELLING OF N-TYPE SUPERLATTICE DETECTOR SYSTEMS WITH USING EMPIRICAL PSEUDOPOTENTIAL METHOD

DISSERTATION

KAZIM AKEL

ESKISEHIR, 2023

BAND MODELLING OF N-TYPE SUPERLATTICE DETECTOR SYSTEMS WITH USING EMPIRICAL PSEUDOPOTENTIAL METHOD

Kazım AKEL

PhD Dissertation

Department of Physics

Programme in Solid State Physics

Supervisor: Prof. Dr. Yüksel ERGÜN

Eskişehir

Eskişehir Technical University

Institute of Graduate Programs

June 2023

FINAL APPROVAL FOR THESIS

This thesis titled BAND MODELLING OF N-TYPE SUPERLATTICE DETECTOR SYSTEMS WITH USING EMPIRICAL PSEUDOPOTENTIAL METHOD has been prepared and submitted by Kazım AKEL in partial fulfillment of the requirements in "Eskişehir Technical University Directive on Graduate Education and Examination" for the Degree of PhD in Physics Department has been examined and approved on 12/06/2023.

Committee Members		**Title, Name and Surname**	**Signature**
Member	:	Prof. Dr. Abidin KILIC	
Member	:	Prof. Dr. Mustafa HOSTUT	
Member	:	Prof. Dr. Cem YÜCE	
Member	:	Prof. Dr. Hüseyin SARI	
Member	:	Doç. Dr. Neslihan ŞAHİN	

Prof. Dr. Semra KURAMA
Director of the Institute of Graduate Programs

12/06/2023

SUPERVISOR APPROVAL

PhD student Kazım AKEL, whom I supervise, has completed this thesis titled BAND MODELLING OF N-TYPE SUPERLATTICE DETECTOR SYSTEMS WITH USING EMPIRICAL PSEUDOPOTENTIAL METHOD. According to my inspections, the work is scientifically and ethically appropriate for the student to the thesis defense exam.

Supervisor
Prof. Dr. Yüksel ERGÜN

ABSTRACT

BAND MODELLING OF N-TYPE SUPERLATTICE DETECTOR SYSTEMS WITH USING EMPIRICAL PSEUDOPOTENTIAL METHOD

Kazım AKEL

Department of Physics

Programme in Solid State Physics

Eskişehir Technical University, Institute of Graduate Programs, June 2023

Supervisor: Prof. Dr. Yüksel ERGÜN

There are high performance infrared superlattice photodedector structures as nBn (J. B. Rodriguez, 2007) dedectors, M-structured (P. Y. Delaunay, 2009) dedectors, W-structured (C. L. Canedy, 2007) dedectors, Complementary barrier infrared detectors (CBIRD) (David Z.-Y. Ting, 2009) , PbIbN (P: p-tipi materyal, N n-tipi materyal, b: bariyer, I: intrinsic [saf, katkısız yarıiletken]) -structured (N. Gautam, 2010) dedectors and N-structred (Ergun & Aydinli, 2012) dedectors taken place in the literature by my Supervisor as a new design. This structure based on a type-II superlattice pin diode is designed for investigating the e-hh wave function overlap functions under reverse bias (U. Kaya, 2013). The structure is called N-structure on the base of real space band profile of $GaSb/AlSb/InAs$ superlattice system. As long as band gap energies of the system has been calculated according to layer thickness correctly with First Principle Method which our team work before (U. Kaya, 2013); pseudo-potentials calculations with plane wave approach have to be done since Bloch functions of the system may not be calculated correctly with First Principle. Especially in 8-12atmospheric window monolayers are more, then, First Principle Calculations take a lot of time and also the absorption and scattering (electron - phonon) processes leads to calculations may not being correctly. For this reason, band calculations are necessary by using Empirical Pseudopotential Method (EPM). In this thesis $InAs/AlSb/GaSb$ type-II superlattice based new detector structure working in the (8-12 μm) atmospheric windows will be designed. Local terms related bulk band structure, band gap and effective mass values will be done in the most accurate way in different temperatures by using EPM.

Keywords: Pseudopotentials, N-type Dedectors, LWIP

ÖZET

"EMPIRICAL PSEUDOPOTENTIAL" METODU KULLANILARAK N-TİPİ SÜPERÖRGÜ DEDEKTÖR SİSTEMLERİNİN BAND MODELLEMESİ

Kazım AKEL

Fizik Anabilim Dalı

Katı Hal Fiziği Bilim Dalı

Eskişehir Teknik Üniversitesi, Lisansüstü Eğitim Enstitüsü, Haziran 2023

Danışman: Prof. Dr. Yüksel ERGÜN

Yüksek performanslı kızılötesi süperörgülü fotodedektör yapılar, nBn (J. B. Rodriguez, 2007) dedektörler, M-yapılı (P. Y. Delaunay, 2009) dedektörler, W-yapılı dedektörler (C. L. Canedy, 2007), Complementary barrier infrared detector (CBIRD) yapılar (David Z.-Y. Ting, 2009) ve PbIbN (P: p-tipi materyal, N n-tipi materyal, b: bariyer, I: intrinsic [saf, katkısız yarıiletken]) yapılı dedektörler (N. Gautam, 2010) ve literature yeni bir tasarım olarak danışmanım tarafından kazandırılan N-yapılı dedektörler (Ergun & Aydinli, 2012) şeklinde yer almaktadırlar. Bu yapı pin dizininin ozellikle Tip-II süperörgü sistemlerinin negatif dış alan altında (reverse bias) e-hh dalga fonksiyonlarinin birlikte var olma dağılımının incelenmesi ile geliştirilmiştir (U. Kaya, 2013). $GaSb/AlSb/InAs$ süperörgü dedektör sistemi olarak gerçek uzay band profili esas alınarak N- yapılı olarak adlandırılmıştır. Ekibimiz tarafından Fırst Principle hesaplamalar yapılarak yasak enerji aralıkları tabaka kalınlıklarına göre doğru hesaplanmış olsa da (U. Kaya, 2013), sistemin Bloch fonksiyonları doğru hesaplanamadığından, düzlem dalga yaklaşımı ile yapay-potansiyeller kullanılarak hesaplamalar yapılması zorunluluğu doğmuştur. Özellikle 8-12 atmosferik pencerede mono tabakaların fazla olması, First Principle hesaplamaların çok fazla zaman almasına ve ayrıca soğrulma ve saçılma (elektron - fonon) proseslerinin doğru hesaplanmamasına neden olmaktadır (yakınsama sorunlarından ötürü). Bu nedenle yapay potansiyel tekniği (EPM) kullanılarak band hesaplamaları yapmak bir zorunluluk olmuştur. Bu tezde, (8-12 μm) atmosferik pencerede çalışan $InAs/AlGaSb/GaSb$ süperörgü tabanlı yeni bir dedektör yapısı tasarlanacak, sistemin band hesaplamaları, külçe band yapısı, yasak enerji ve etkin kütle değerlerinin en doğru biçimde hesaplandığı Yapay Potansiyel Tekniği (EPM) kullanılarak yapılacaktır.

Anahtar Sözcükler: Yapay Potansiyeller, N-Tipi Dedektörler, LWIP

ACKNOWLEDGEMENTS

First of all, I do want to express my thanks to my doctoral advisor Professor Yuksel Ergun for his careful and continuous guidance and intense help during this work. As a renowned physicist in the field of theoretical solid-state physics he always has been a role model in my life and taught me how to enjoy learning and doing research. I have been adorabubble lucky to study with him and I am in hopes of that one day I would become as good an advisor to my students as he has been to me.

I would like to thank my dissertation committee members, Prof. Dr. Mustafa HOSTUT, Prof. Dr. Abidin KILIC, Prof. Dr. Cem YUCE, Prof. Dr. Hüseyin SARI, Doç. Dr. Neslihan SAHIN for their sincere interest and creative criticism, offer and recommendation for this work.

Finally, and most importantly, I thank to my wife Yurda and my children Ozgur and Arya for their limitless toleratıon, backing and favor during all these years. Without their love and support, this dissertation would not have been probable.

Kazım AKEL

12/06/2023

STATEMENT OF COMPLIANCE WITH ETHICAL PRINCIPLES AND RULES

I hereby truthfully declare that this thesis is an original work prepared by me; that I have behaved in accordance with the scientific ethical principles and rules throughout the stages of preparation, data collection, analysis and presentation of my work; that I have cited the sources of all the data and information that could be obtained within the scope of this study, and included these sources in the references section; and that this study has been scanned for plagiarism with "scientific plagiarism detection program" used by Eskişehir Technical University, and that "it does not have any plagiarism" whatsoever. I also declare that, if a case contrary to my declaration is detected in my work at any time, I hereby express my consent to all the ethical and legal consequences that are involved.

Kazım AKEL

CONTENTS

Page

LIST OF TABLES

Page

LIST OF FIGURES

Page

GLOSSARY OF SYMBOLS AND ABBREVIATIONS

EPM	:	Empirical Pseudopotential Method
SEPM	:	Superlattice Empirical Pseudopotential Method
LWIP	:	Long Wave Infrared Photodedector
SWIP	:	Short Wave Infrared Photodedector
MWIP	:	Mid Wave Infrared Photodedector
CBIRD	:	Complementary Barrier Infrared Detectors
OPW	:	Orthogonalized Plane-Wave
WS	:	Wigner-Seitz
T2SL	:	Type II Superlattice
FCC	:	Face-Centered Cubic
ML	:	Monolayer
T2SL	:	Type II Superlattice
FCC	:	Face-Centered Cubic

1. INTRODUCTION

E. Fermi introduced the first pseudopotential method in 1934 (Fermi, 1934) to study high lying atomic levels. Later this pseudopotential method used by Hellman to calculate energy levels of alkali metals (Hellmann, 1935).

We use the effective pseudopotential with respect to real potential between the core electrons and nucleus. Then we write the effective pseudopotential instead of real Coulomb potential in Hamiltonian of the Schrödinger equation. With this approximation we compress the core states and remove from the calculations. Therefore we built a new potential which describe all electrons of atoms which named pseudopotential. This result permits the pseudo wavefunctions to define with less Fourier modes. Thus using plane-wave basis sets are practical. With pseudopotential method because of the core states removed from the calculation, we are interested in the only active valance electrons. The Fig.1.1 schematically shows a classic electron conduction band wave function (Böer & Pohl, 2017) . For out of a cut-off distance (outside of the ion core) which we denote here such that r_c, the real eigenstates have the same energy with the pseudo states.

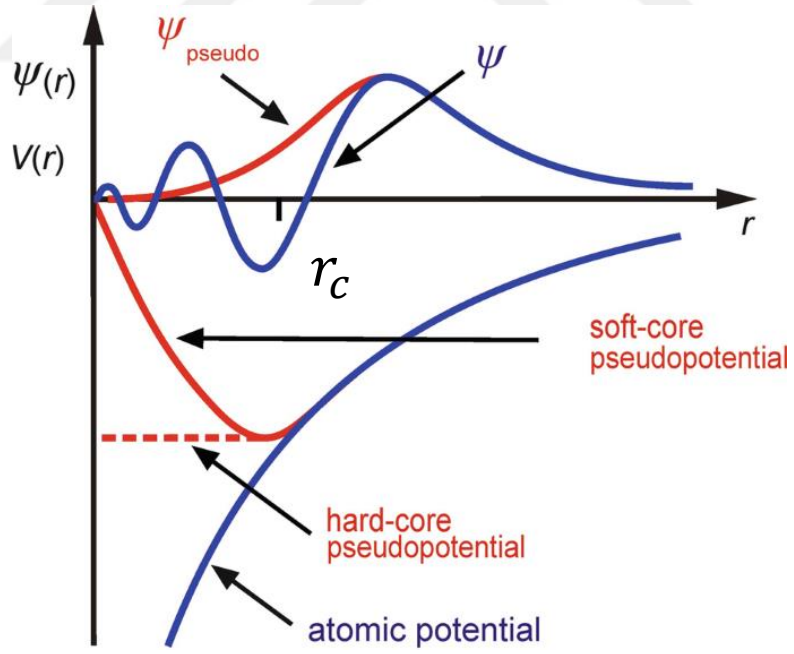

Figure 1.1. *The blue curve shows the real atomic Coulomb potential and the dashed red curve shows hard core pseudopotential and the solid red curve shows soft core pseudopotential (Böer & Pohl, 2017).*

We don’t have any information about the core electrons with using pseudopotential instead of the real lattice potential but for semiconductors this is not too important. Nevertheless, advance of the simplicity of describing the solutions with pseudowavefunctions approached more easily by superposition of less terms. The resulting eigenvalues for the valence and conduction bands, however, are the same as obtained with the exact potential extending into the core region.

In Empirical Pseudopotential Method (EPM) we can get the results with repeated readjustment of the pseudopotential in iterative trials as discussed. The Empirical Pseudopotential Method (EPM) determines a bulk solid potential with fitting the band structure, which we have from experiment. When you fitted the parameters from empirically, the understanding that can be succeeded between theory and experiment is rather good.

2. BAND STRUCTURE AND PSEUDOPOTENTIALS

2.1. Theoretical Background of EPM

Which is one of the common model of material relating atoms model describe a collection of discrete atoms to a model of a material composed of cores holding periodically arranged nuclei with their core electrons and a sea of valence electrons interacting with the positive cores and each other (Cohen, Nanotubes, nanoscience, and nanotechnology, 2011) (Cohen & Chelikowsky, Electronic Structure and Optical Properties of Semiconductors, 1988). With describing pseudopotential theory, core electrons approximation assumes they are taken to be unperturbed w.r.t. the equation of the material. Therefore, the cores in materials are frozen as the same as the cores in remote atoms with only the valence electrons readjust as the material is formed. In an ideal world, the whole Hamiltonian for a crystal includes relativistic effects with kinetic energies of core-core, electron-core; electron-electron Coulomb interactions. Nevertheless, in practice it is impossible to study this all interactions for the crystal so we use much simplifications and approximations to solve the Hamiltonian equation. Assumes the electrons follows the core motion 'adiabatically' which is adiabatic approximation (or Born-Oppenheimer approximation) permits us to decouple the core and electron parts of the whole Hamiltonian. Since we interest the structure of band profile E($\vec{k}$) calculation, here we can more simplify the problem by discounting the core motion like frozen-cores. So, the whole Hamiltonian can be written as;

$$H = \sum_i \frac{{p_i}^2}{2m} + \sum_{i \neq j} \frac{e^2}{4\pi\varepsilon_0 |\vec{r_i} - \vec{r_j}|} + \sum_{i,\alpha} V_\alpha(\vec{r}_i - \vec{R}_\alpha) \qquad (2.1)$$

which the indices i and j denote to electrons and α denotes to cores and $\vec{r}_i$ and $\vec{R}_\alpha$ symbolize the coordinates of electrons and cores, respectively. In Eqn.2.1 the first term of the right-hand side is kinetic energy of the electrons; the second term of the right-hand side is electron-electron Coulomb interactions and the last term of the right-hand side in the Eqn.2.1 is electron-core Coulomb interaction V_α. But, the many body problem in Eqn.2.1 is still unsolvable therefore we necessity additional simplification in the above equation. The Hartree (mean field) approximations studies on the one electron and assumes that each electron moves in the average field which generated by all the other

electrons. Then the whole Hamiltonian can be show as the sum of one electron Hamiltonians;

$$H = \sum_i H_i \tag{2.2}$$

which is the one electron Hamiltonian H_i s.t.

$$H_i = \frac{{p_i}^2}{2m} + \sum_j \frac{e^2}{4\pi\varepsilon_0} \int \frac{\psi_j^*(\vec{r_j})\psi_j(\vec{r_j})}{|\vec{r_i} - \vec{r_j}|} d\vec{r} + \sum_\alpha V_\alpha(\vec{r_i} - \vec{R}_\alpha) \tag{2.3}$$

Here the integral term in the right-hand side in Eqn.2.3 represents the electrostatic potential of the charge density of the j^{th} electrons, therefore the second term of the Eqn.2.3 creates the 'mean field' due to all other electrons. So, the electronic wavefunctions are product of one-electron wavefunctions and the Pauli principle should be obeyed. So, with using the Hartree approximation we can rewrite the Eq.2.3 as follows,

$$H_i = \frac{{p_i}^2}{2m} + V_{lat}(\vec{r}) \tag{2.4}$$

Here the function $V_{lat}(\vec{r})$ includes the electron-electron and electron-core Coulomb interactions together. Clearly, we want to determine the $V_{lat}(\vec{r})$ term in Eqn.2.4 for $E_n(\vec{k})$ and $\psi_n(\vec{r})$ with solving the Schrödinger's equation. Here $E_n(\vec{k})$ and $\psi_n(\vec{r})$ can be simplified with advantage of the translational symmetry in a crystal structure.

By the derivation of the pseudopotential theory; we assume that the core electrons frozen in the atoms. So, we consider the valence electrons which they responsible to the atomic bonding, they move in a weak single electron potential. The concept of the pseudopotential theory started from the orthogonalized plane wave (OPW) method. In the OPW method the single electron wavefunctions developed over the subset of plane waves are orthogonal to the core states. After that Phillips and Kleinman use their cancellation theorem (Phillips & Kleinman, 1959) to derive the formulation of the pseudopotential theory. Here we start with the mathematical formulation of Phillips and Kleinman as below. We assume that the accurate crystal wavefunction ψ equal to the sum of ϕ which is the smooth wavefunction and sum over as a sum of a smooth wavefunction ϕ and a sum over occupied core states ξ_t for a discrete ion as below:

$$\psi = \phi + \sum_t c_t \xi_t \tag{2.5}$$

Here we can assume that with using OPW method ψ is orthogonal to the core states. This means that $\langle \xi_t | \psi \rangle = 0$, then the coefficients c_t in the Eqn.2.5 can be written as,

$$c_t = -\langle \xi_t | \phi \rangle \tag{2.6}$$

So, we can write the Eqn.2.5 s.t.

$$\psi = \phi - \sum_t \langle \xi_t | \phi \rangle \xi_t \tag{2.7}$$

Here we want to write the Hamiltonian with using the Schrödinger's equation, $H = \hat{p}^2/2m + V_c$ which is operating on ψ. If we substitute the Eqn.2.7 into the $H\psi = E\psi$, then we can get Eqn.2.8 s.t.

$$H\psi = H\phi - \sum_t E_t |\xi_t\rangle \langle \xi_t | \phi \rangle = E\psi \tag{2.8}$$

Here we substitute again the Eqn.2.7 into the second right hand side of the Eqn.2.8 than we get;

$$H\phi + \sum_t (E - E_t) \xi_t \langle \xi_t | \phi \rangle = E\phi \tag{2.9}$$

If we simplify the Eqn.2.9 s.t.,

$$(H + V_{nl})\phi = E\phi \tag{2.10}$$

We write V_{nl} which is the nonlocal pseudopotential s.t.

$$V_{nl}\phi = \sum_t (E - E_t) \xi_t \langle \xi_t | \phi \rangle \tag{2.11}$$

Now if we the Hamiltonian H which includes the kinetic and potential parts in Eqn.2.10, we get;

$$\left[-\frac{\hbar^2}{2m}\nabla^2 + V_c + V_{nl}\right]\phi = \left[-\frac{\hbar^2}{2m}\nabla^2 + V_{pseudo}\right]\phi = E\phi \qquad (2.12)$$

In Eqn.2.12, we use the V_{pseudo} which we named it pseudopotential. The pseudopotential V_{pseudo} is the sum of long ranged core and short ranged nonlocal potentials (Bester, 2009). We know that the Eq.2.12 is called pseudopotential equation which we can obtain exact pseudo wavefunction ϕ outside the cores. Here we know that the energy E in the Eqn.2.12 gives us the eigenvalues of the exact wavefunction ψ.

After this point, we try to find the pseudopotential $V_{pseudo}(\vec{r})$ in the Eqn.2.12. this pseudopotential gives correct wavefunctions outside the cores. The Fourier transform of the pseudopotential $V_{pseudo}(\vec{r})$ in the reciprocal space is $V(\vec{G})$. In the Empirical Pseudopotential Method, we fit the $V(\vec{G})$'s with using the band structure of an element which comes experimentally. In the following sections we defined this method.

2.2. Empirical Pseudopotential Method for Bulk Solids

In the section 2.2 we described the Local Empirical Pseudopotential Method to get the band profile of the bulk solids. The commonly used method was introduced by Chelikowsky and Cohen (Chelikowsky & Cohen, 1974) (J.R. & M.L., 1976).

We start to write the total Hamiltonian of a solid with sum of Local, NonLocal and Spin Orbit terms s.t.

$$H^{TOT}_{\vec{G},\vec{G}'} = H^{L}_{\vec{G},\vec{G}'} + H^{NL}_{\vec{G},\vec{G}'} + H^{SP}_{\vec{G},\vec{G}'} \qquad (2.13)$$

Here the Local part of the total Hamiltonian in Eqn.2.13 $H^{L}_{\vec{G},\vec{G}'}$ is used to solve the single electron Schrödinger equation. So, we can write the Local part as follows;

$$H^{L}_{\vec{G},\vec{G}'}\psi(\vec{r}) = -\frac{\hbar^2}{2m}\nabla^2\psi(\vec{r}) + V_{lat}(\vec{r})\psi(\vec{r}) = E_{\vec{k}}\psi(\vec{r}) \qquad (2.14)$$

Here the function $V_{lat}(\vec{r})$ describe the periodic lattice potential s.t. $V_{lat}(\vec{r}) = V_{lat}(\vec{r} + \vec{r}')$. But here we must note that we ignore the nonlocal potential effects. If we know that the $V_{lat}(\vec{r})$ function is periodic; we can write the wave function as a Bloch function s.t.

$$\begin{aligned}\psi_{\vec{k}}(\vec{r}) &= e^{i\vec{k}\vec{r}} \sum_{\vec{G}} u_{\vec{k},\vec{G}} e^{i\vec{G}.\vec{r}} \\ &= \sum_{\vec{G}} u_{\vec{k},\vec{G}} e^{i(\vec{k}+\vec{G}).\vec{r}} \\ &= \sum_{\vec{G}} u_{\vec{k}+\vec{G}} e^{i(\vec{k}+\vec{G}).\vec{r}}\end{aligned} \tag{2.15}$$

Here we can note that the $\vec{G}$ vectors are the reciprocal lattice vectors. So, if we write the Eqn.2.15 into the Eq.2.14 we get,

$$\begin{aligned}-\frac{\hbar^2}{2m}\nabla^2\psi(\vec{r}) &= -\frac{\hbar^2}{2m}\nabla^2\left[\sum_{\vec{G}} u_{\vec{k}+\vec{G}} e^{i(\vec{k}+\vec{G}).\vec{r}}\right] \\ &= -\frac{\hbar^2}{2m}\sum_{\vec{G}} u_{\vec{k}+\vec{G}}\left[\nabla^2 e^{i(\vec{k}+\vec{G}).\vec{r}}\right] \\ &= \frac{\hbar^2}{2m}\sum_{\vec{G}} u_{\vec{k}+\vec{G}}\left[\left|\vec{k}+\vec{G}\right|^2 e^{i(\vec{k}+\vec{G}).\vec{r}}\right]\end{aligned} \tag{2.16}$$

In Eq.2.16 ∇^2 is the second order derivative of a vector function w.r.t. $\vec{r}$, so we get third step of Eq.2.16. Here if we use the Fourier transform of the local Hamiltonian then we get,

$$\begin{aligned}&\frac{\hbar^2}{2m}\sum_{\vec{G}}\left|\vec{k}+\vec{G}\right|^2 u_{\vec{k}+\vec{G}}\, e^{i(\vec{k}+\vec{G}).\vec{r}} \\ &\quad + V_{lat}(\vec{r})\sum_{\vec{G}} u_{\vec{k}+\vec{G}}\, e^{i(\vec{k}+\vec{G}).\vec{r}} = E(\vec{k})\sum_{\vec{G}} u_{\vec{k}+\vec{G}}\, e^{i(\vec{k}+\vec{G}).\vec{r}}\end{aligned} \tag{2.17}$$

Now we can multiply both hand sides of the Eqn.2.17 by $e^{-i(\vec{k}+\vec{G}').\vec{r}}$, then we get,

$$\begin{aligned}&\frac{\hbar^2}{2m}\sum_{\vec{G}}\left|\vec{k}+\vec{G}\right|^2 u_{\vec{k}+\vec{G}}\, e^{i(\vec{G}-\vec{G}').\vec{r}} \\ &\quad + V_{lat}(\vec{r})\sum_{\vec{G}} u_{\vec{k}+\vec{G}}\, e^{i(\vec{G}-\vec{G}').\vec{r}} = E(\vec{k})\sum_{\vec{G}} u_{\vec{k}+\vec{G}}\, e^{i(\vec{G}-\vec{G}').\vec{r}}\end{aligned} \tag{2.18}$$

If we take the integration of both sides of Eqn.2.18 w.r.t. whole volume of the solid, then the first term of the left-hand side in Eqn.2.18 turn into,

$$\frac{\hbar^2}{2m}\int_{-\infty}^{\infty}\sum_{\vec{G}}\left|\vec{k}+\vec{G}\right|^2 u_{\vec{k}+\vec{G}}\, e^{i(\vec{G}-\vec{G}').\vec{r}}\, d^3\vec{r}$$

$$= \frac{\hbar^2}{2m}\sum_{\vec{G}}\left|\vec{k}+\vec{G}\right|^2 u_{\vec{k}+\vec{G}} \underbrace{\int_{-\infty}^{\infty} e^{i(\vec{G}-\vec{G}').\vec{r}}\, d^3\vec{r}}_{(a)} \tag{2.19}$$

$$= (2\pi)^3\, \frac{\hbar^2}{2m}\sum_{\vec{G}}\left|\vec{k}+\vec{G}\right|^2 u_{\vec{k}+\vec{G}}\, \underbrace{\delta\left(\vec{G}-\vec{G}'\right)}_{(b)}$$

$$= (2\pi)^3\, \frac{\hbar^2}{2m}\left|\vec{k}+\vec{G}'\right|^2 u_{\vec{k}+\vec{G}'}$$

$$(a)\quad \overset{from\ the\ Fourier\ Transform}{\int_{-\infty}^{\infty} e^{i(\vec{G}-\vec{G}').\vec{r}}\, d^3\vec{r} = (2\pi)^3\delta\left(\vec{G}-\vec{G}'\right)} \tag{2.20}$$

$$(b)\quad \overset{Kronikher\ Delta\ Function}{\delta\left(\vec{G}-\vec{G}'\right) = \begin{cases}1, & \vec{G}=\vec{G}'\\ 0, & Otherwise\end{cases}} \tag{2.21}$$

the second term of the left-hand side would be,

$$\int_{-\infty}^{\infty} V_{lat}(\vec{r})\sum_{\vec{G}} u_{\vec{k}+\vec{G}}\, e^{i(\vec{G}-\vec{G}').\vec{r}}\, d^3\vec{r}$$

$$= \sum_{\vec{G}} u_{\vec{k}+\vec{G}} \int_{-\infty}^{\infty} V_{lat}(\vec{r})\, e^{i(\vec{G}-\vec{G}').\vec{r}}\, d^3\vec{r} \tag{2.22}$$

$$= \sum_{\vec{G}} u_{\vec{k}+\vec{G}}\, V\left(\vec{G}-\vec{G}'\right)(2\pi)^3$$

where;

$$H^L_{\vec{G},\vec{G}'}\psi(\vec{r}) = -\frac{\hbar^2}{2m}\nabla^2\psi(\vec{r}) + V_{lat}(\vec{r})\psi(\vec{r}) = E_{\vec{k}}\psi(\vec{r}) \tag{2.23}$$

and the right-hand side of Eqn.2.18 would be,

$$E(\vec{k})\sum_{\vec{G}} u_{\vec{k}+\vec{G}}\int_{-\infty}^{\infty} e^{i(\vec{G}-\vec{G}').\vec{r}}\, d^3\vec{r} \;=\; E(\vec{k})\sum_{\vec{G}} u_{\vec{k}+\vec{G}}\,(2\pi)^3\delta\left(\vec{G}-\vec{G}'\right)$$

$$= (2\pi)^3\, E\left(\vec{k}\right) u_{\vec{k}+\vec{G}'} \tag{2.24}$$

again with using Fourier Transform in Eqn.2.20. Thus, we can write the Eqn.2.18 such that,

$$(2\pi)^3 \frac{\hbar^2}{2m} \left|\vec{k}+\vec{G}'\right|^2 u_{\vec{k}+\vec{G}'} + \sum_{\vec{G}} u_{\vec{k}+\vec{G}} V(\vec{G}-\vec{G}')(2\pi)^3 = (2\pi)^3 E(\vec{k}) u_{\vec{k}+\vec{G}'} \tag{2.25}$$

If we can simplify both side with $(2\pi)^3$, then we get;

$$\frac{\hbar^2}{2m} \left|\vec{k}+\vec{G}'\right|^2 u_{\vec{k}+\vec{G}'} + \sum_{\vec{G}} u_{\vec{k}+\vec{G}} V(\vec{G}-\vec{G}') = E(\vec{k}) u_{\vec{k}+\vec{G}'} \tag{2.26}$$

then we can multiply by $\sum_{\vec{G}} \delta(\vec{G}-\vec{G}')$ to the first term of left- and right-hand sides of Eqn.2.26,

$$\sum_{\vec{G}} \frac{\hbar^2}{2m} \left|\vec{k}+\vec{G}'\right|^2 u_{\vec{k}+\vec{G}'} \delta(\vec{G}-\vec{G}') + \sum_{\vec{G}} u_{\vec{k}+\vec{G}} V(\vec{G}-\vec{G}') = \sum_{\vec{G}} E(\vec{k}) u_{\vec{k}+\vec{G}'} \delta(\vec{G}-\vec{G}') \tag{2.27}$$

where $\sum_{\vec{G}} \delta(\vec{G}-\vec{G}') = V$ and $\delta(\vec{G}-\vec{G}') = 1$ if $\vec{G} = \vec{G}'$. We called this equation s.t. homogeneous linear equation. So, we can write this s.t.

$$\sum_{\vec{G}} \left[\left(\frac{\hbar^2}{2m} \left|\vec{k}+\vec{G}'\right|^2 - E(\vec{k}) \right) \delta(\vec{G}-\vec{G}') + V(\vec{G}-\vec{G}') \right] \boldsymbol{u}_{\vec{k}+\vec{G}} = \underline{\mathbf{0}} \tag{2.28}$$

This homogeneous linear equation can be written as;

$$A\underline{\boldsymbol{x}} = \underline{\mathbf{0}} \tag{2.29}$$

Here the matrix A represent the matrix form of the sum term in Eqn.2.28, the vector $\underline{\boldsymbol{x}}$ represent the vector form of $\boldsymbol{u}_{\vec{k}+\vec{G}'}$ and $\underline{\mathbf{0}}$ is the zero vector. Homogeneous linear equations have nontrivial (nonzero) solutions if and only if the determinant of the matrix A is equal zero. Thus, for the solution of the Eqn.2.28 we must calculate;

$$Det \left| \left(\frac{\hbar^2}{2m} \left|\vec{k}+\vec{G}'\right|^2 - E(\vec{k}) \right) \delta(\vec{G}-\vec{G}') + V(\vec{G}-\vec{G}') \right| = 0 \tag{2.30}$$

The term $V(\vec{G}-\vec{G}')$, which we write in Eqn.2.23, can be simplified using its periodicity of the potential. We can assume that the wavefunctions are normalized over

the volume of the solid V. Here we can say in the wigner-seitz (WS) cell, the sum of the ionic potential is $V_{lat}(\vec{r})$. Here we use some indices in each cell s.t. the indices $l, m, \ldots$ using for cells and $\alpha, \beta \ldots$ for ions. So, in a position $\vec{r}$ the lattice potential $V_{lat}(\vec{r})$ can be written as a linear superposition of V_{ion}, which is the ionic potential s.t.

$$V_{lat}(\vec{r}) = \sum_{l,\alpha} V_{ion}(\vec{r} - \vec{R}_l - \vec{\tau}_\alpha) \tag{2.31}$$

As we write above the V_{ion} is the ionic potential of the specific ion $\vec{\tau}_\alpha$ in the cell at the position $\vec{R}_l$. Therefore if we substitute Eqn.2.31 in to the Eqn.2.23, we can write the Eqn.2.23 s.t.,

$$V(\vec{G} - \vec{G}') = \frac{1}{V} \int_V \sum_{l,\alpha} V_{ion}(\vec{r} - \vec{R}_l - \vec{\tau}_\alpha)\ e^{i(\vec{G}-\vec{G}').\vec{r}}\ d^3\vec{r} \tag{2.32}$$

Let $\vec{r}' = \vec{r} - \vec{R}_l - \vec{\tau}_\alpha$ as new integration variable, then

$$\begin{aligned} V(\vec{G} - \vec{G}') &= \frac{1}{V} \sum_{l,\alpha} \int_V V_{ion}(\vec{r}')\ e^{i(\vec{G}-\vec{G}').(\vec{r}'+\vec{R}_l+\vec{\tau}_\alpha)}\ d^3\vec{r}' \\ &= \frac{1}{V} \sum_{l,\alpha} e^{i(\vec{G}-\vec{G}').\vec{R}_l} e^{i(\vec{G}-\vec{G}').\vec{\tau}_\alpha} \int_V V_{ion}(\vec{r}')\ e^{i(\vec{G}-\vec{G}').\vec{r}'}\ d^3\vec{r}' \\ &= \frac{1}{V} \sum_{l} e^{i(\vec{G}-\vec{G}').\vec{R}_l} \sum_{\alpha} e^{i(\vec{G}-\vec{G}').\vec{\tau}_\alpha} \int_V V_{ion}(\vec{r}')\ e^{i(\vec{G}-\vec{G}').\vec{r}'}\ d^3\vec{r}' \end{aligned} \tag{2.33}$$

We know that the ionic potential $V_{ion}(\vec{r})$ is short range, so we can assume that this potential can neglect the integral part of Eqn.2.33 outside the WS cell. Then the integral part of Eqn.2.33 becomes,

$$\int_V V_{ion}(\vec{r}')\ e^{i(\vec{G}-\vec{G}').\vec{r}'}\ d^3\vec{r}' = \int_\Omega V_{ion}(\vec{r}')\ e^{i(\vec{G}-\vec{G}').\vec{r}'}\ d^3\vec{r}' \tag{2.34}$$

In Eqn.2.34, we denote Ω as the volume of WS cell. Here we also note that;

$$\sum_{l} e^{i(\vec{G}-\vec{G}').\vec{R}_l} = \sum_{l} 1 = N_{cell} \tag{2.35}$$

Which N_{cell} denote the number of cells in the volume of V, so we can write;

$$e^{i(\vec{G}-\vec{G}').\vec{R}_l} = e^{i2n\pi} = 1 \tag{2.36}$$

Here we can show that,

$$\begin{aligned} V(\vec{G}-\vec{G}') &= \frac{N_{cell}}{V}\sum_{\alpha} e^{i(\vec{G}-\vec{G}').\vec{\tau}_\alpha}\int_{\Omega} V_{ion}(\vec{r}')\, e^{i(\vec{G}-\vec{G}').\vec{r}'}\, d^3\vec{r}' \\ &= \frac{N_{cell}}{V}\sum_{\alpha} e^{i(\vec{G}-\vec{G}').\vec{\tau}_\alpha}\frac{\Omega}{\Omega}\int_{\Omega} V_{ion}(\vec{r}')\, e^{i(\vec{G}-\vec{G}').\vec{r}'}\, d^3\vec{r}' \\ &= \frac{N_{cell}\Omega}{V}\sum_{\alpha} e^{i(\vec{G}-\vec{G}').\vec{\tau}_\alpha}\frac{1}{\Omega}\int_{\Omega} V_{ion}(\vec{r}')\, e^{i(\vec{G}-\vec{G}').\vec{r}'}\, d^3\vec{r}' \\ &\approx S(\vec{G}-\vec{G}')V_{ion}(\vec{G}-\vec{G}') \end{aligned} \tag{2.37}$$

Here the terms $V_{ion}(\vec{G}-\vec{G}')$ and $S(\vec{G}-\vec{G}')$ are called atomic form factor and structure factor respectively. $V_{ion}(\vec{G}-\vec{G}')$ is the Fourier transform of atomic potential and $S(\vec{G}-\vec{G}')$ is the location of the ions within given WS cell.

$$V_{ion}(\vec{G}-\vec{G}') = \frac{1}{\Omega}\int_{\Omega} V_{ion}(\vec{r}')\, e^{i(\vec{G}-\vec{G}').\vec{r}'}\, d^3\vec{r}' \tag{2.38}$$

$$S(\vec{G}-\vec{G}') = \frac{1}{N}\sum_{\alpha} e^{i(\vec{G}-\vec{G}').\vec{\tau}_\alpha} \tag{2.39}$$

Here if we specialized the Eqn.2.38 and 2.39 for a zinc blende structure then we know that we have just two ions in a unit cell at the positions $\vec{\tau}_1 = (0,0,0)$ and $\vec{\tau}_2 = a_0\frac{1}{4}(1,1,1)$. Here a_0 is the unstrained lattice constant which differ for any bulk solids. Therefore, we can easily simplify the atomic form factors for two ions in a cell s.t.

$$V(\vec{G}-\vec{G}') = V_{\vec{G}\vec{G}',1}e^{i(\vec{G}-\vec{G}').\vec{\tau}_1} + V_{\vec{G}\vec{G}',2}e^{i(\vec{G}-\vec{G}').\vec{\tau}_2} \tag{2.40}$$

To the simplification, we can move the origin of the coordinate to the mid-point of the ions, then we can write $\vec{\tau}_1 = \vec{\tau} = a_0\frac{1}{8}(1,1,1)$ and $\vec{\tau}_2 = -\vec{\tau} = -a_0\frac{1}{8}(1,1,1)$. If we write these two vectors in Eqn.2.40 we get,

$$\begin{aligned} V(\vec{G}-\vec{G}') &= V_{\vec{G}\vec{G}',1}e^{i(\vec{G}-\vec{G}').\vec{\tau}} + V_{\vec{G}\vec{G}',2}e^{-i(\vec{G}-\vec{G}').\vec{\tau}} \\ &= V^s(\vec{G}-\vec{G}')\cos\{(\vec{G}-\vec{G}').\vec{\tau}\} + iV^a(\vec{G}-\vec{G}')\sin\{(\vec{G}-\vec{G}').\vec{\tau}\} \\ &= V^s(\vec{G}-\vec{G}')S^s(\vec{G}-\vec{G}') + iV^a(\vec{G}-\vec{G}')S^a(\vec{G}-\vec{G}') \end{aligned} \tag{2.41}$$

where the structure factors are,

$$S^s(\vec{G}-\vec{G}') = \cos\{(\vec{G}-\vec{G}').\vec{\tau}\} \tag{2.42}$$

$$S^a(\vec{G}-\vec{G}') = \sin\{(\vec{G}-\vec{G}').\vec{\tau}\} \tag{2.43}$$

So here we can write the symmetric $V^s_{|\vec{G}-\vec{G}'|}$ and asymmetric form factor $V^a_{|\vec{G}-\vec{G}'|}$ s.t.

$$V^s_{|\vec{G}-\vec{G}'|} = \frac{1}{2}(V_{\vec{G}\vec{G}',1} + V_{\vec{G}\vec{G}',2}) \tag{2.44}$$

$$V^a_{|\vec{G}-\vec{G}'|} = \frac{1}{2}(V_{\vec{G}\vec{G}',1} - V_{\vec{G}\vec{G}',2}) \tag{2.45}$$

Which atomic pseudopotential of a zinc blende structure that have two ions in the cell is s.t.

$$V_{\vec{G}\vec{G}',i} = \frac{2}{\Omega}\int_{\Omega} V_i(\vec{r})\, e^{i(\vec{G}-\vec{G}').\vec{r}}\, d^3\,\vec{r} \tag{2.46}$$

Here the indices $i = 1$ and 2 are the anion and cation components for a zinc-blende structure s.t. Si and Ge.

We know that in the local pseudopotential approximation first we fit the symmetric and asymmetric form factors with using the experimental data. By the way we get the correct electronic band profile of a bulk solid and it gives us many physical properties of the crystal.

Classically, we assume that the ionic potential is spherically symmetric, therefore the form factors depend on the magnitude of the reciprocal vector $\vec{G}$ (J.R. & M.L., 1976). Because of the elimination of the strong core potential, the full Fourier transform $V(q) = |\vec{G}-\vec{G}'|$ becomes very weak for q is large enough. So, we just use the form factors, which are the empirical parameters of a bulk solid, is $|\vec{G}-\vec{G}'| = \sqrt{3}$, $\sqrt{8}$ and $\sqrt{11}\; x\; \frac{2\pi}{a_0}$.

In conclusion, we can write linear homogeneous equation in Eqn.2.28 by using form and structure factors s.t.

$$\sum_{\vec{G}}\left[\left(\frac{\hbar^2}{2m}\left|\vec{k}+\vec{G}'\right|^2 - E(\vec{k})\right)\delta_{\vec{G},\vec{G}'} + V^s_{\vec{G},\vec{G}'}S^s_{\vec{G},\vec{G}'} + iV^a_{\vec{G},\vec{G}'}S^a_{\vec{G},\vec{G}'}\right]\boldsymbol{u}_{\vec{k}+\vec{G}} = \underline{\mathbf{0}} \tag{2.47}$$

Therefore, now we can write the well-known equation of Eqn.2.30 which gives us the eigenvalue problem s.t.

$$Det\left|\left(\frac{\hbar^2}{2m}\left|\vec{k}+\vec{G}'\right|^2 - E(\vec{k})\right)\delta_{\vec{G},\vec{G}'} + V^s_{\vec{G},\vec{G}'}S^s_{\vec{G},\vec{G}'} + iV^a_{\vec{G},\vec{G}'}S^a_{\vec{G},\vec{G}'}\right| = 0 \qquad (2.48)$$

With using Eqn.2.48 we build linear equation in the matrix form w.r.t. reciprocal lattice vector $\vec{G}$ and , $\vec{G}'$. This matrix has the diagonal terms s.t. $\frac{\hbar^2}{2m}\left|\vec{k}+\vec{G}'\right|^2$. Here we want to get the eigenvalues $E(\vec{k})$ and these eigenvalues gives us the energy bands in k space with solving the linear equation in Eqn.48.

2.3. Spin Orbit Interaction for Bulk Solids

We know that the spin orbit interaction can have major importance for the electronic band modelling of any semiconductors. The spin orbit interaction specifically important for the behavior of the electrons near the valence band maximum.

If any solid, pass in an electrostatic field $\vec{e}$ with the velocity $\vec{v}$, the special relativity tells us that the observer has a magnetic field s.t.

$$\vec{B} = -\gamma\vec{\beta}\times\vec{\varepsilon} \qquad (2.49)$$

Which we denote that $\vec{\beta} = \frac{\vec{v}}{c}$ and $\gamma^2 = 1-\vec{\beta}^2$. Therefore, this magnetic field in Eqn.2.49 can re-write s.t.

$$\vec{B} = -\frac{\vec{v}}{c}\times\vec{\varepsilon} = -\frac{\vec{P}}{mc}\times\vec{\varepsilon} \qquad (2.50)$$

This is the nature of the magnetic field with which the magnetic moment of the orbiting valence electron interacts (Liboff, 2003). Put differently, which we known as the spin-orbit interaction is the interaction between the spin induced magnetic moment and the magnetic field. Analytically, we can write the spin-orbit Hamiltonian such that (Saravia & Brust, 1968) (Weisz, 1966),

$$H^{SO} = \frac{\hbar}{4mc^2}(\nabla V\times\hat{p}\cdot\hat{\sigma}) \qquad (2.51)$$

In Eqn.2.51 which V is the lattice potential, $\hat{p}$ is the momentum operator, and $\hat{\sigma}$ is the Pauli spin operator. Chelikowsky et al. (J.R. & M.L., 1976) have included spin-orbit

interactions by extension of a method first presented by Saravia and Brust (Saravia & Brust, 1968) for Ge and have followed the work of Weisz (Weisz, 1966), as modified by Bloom and Bergstresser (Bloom & Bergstresser, 1968).

Here we use and follow Chelikowsky et al. approach (J.R. & M.L., 1976) In this approach they form a 2 by 2 matrix to define the pseudopotential Hamiltonian as follows,

$$H^{SO}_{\vec{G},\vec{G}'} = (\vec{K} \times \vec{K}')\vec{\sigma}_{s,s'}\left[-i\lambda^s cos\{(\vec{G} - \vec{G}') \cdot \vec{\tau}\} + \lambda^a sin\{(\vec{G} - \vec{G}') \cdot \vec{\tau}\}\right] \quad (2.52)$$

Which we write symmetric and antisymmetric factors and Pauli spin vectors;

$$\begin{aligned} \lambda^s &= \frac{1}{2}(\lambda_A + \lambda_B) \\ \lambda^a &= \frac{1}{2}(\lambda_A - \lambda_B) \end{aligned} \quad (2.53)$$

$$\begin{aligned} \lambda_A &= \mu B^A_{nl}(K) B^A_{nl}(K') \\ \lambda_B &= \alpha\mu B^B_{nl}(K) B^B_{nl}(K') \end{aligned} \quad (2.54)$$

$$\vec{\sigma} = \begin{pmatrix} 0 & 1 \\ 1 & 0 \end{pmatrix}\hat{\sigma}_x + \begin{pmatrix} 0 & -i \\ i & 0 \end{pmatrix}\hat{\sigma}_y + \begin{pmatrix} 1 & 0 \\ 0 & -1 \end{pmatrix}\hat{\sigma}_z \quad (2.55)$$

In Eqn.2.56 the matrix vector product $(\vec{K} \times \vec{K}')\vec{\sigma}_{s,s'}$ can be wrote as follows,

$$\begin{aligned} &(\vec{K} \times \vec{K}')\vec{\sigma}_{s,s'} \\ &= \begin{pmatrix} K_1K_2{}' - K_2K_1{}' & (K_2K_3{}' - K_3K_2{}') + i(K_1K_3{}' - K \\ (K_2K_3{}' - K_3K_2{}') + i(K_3K_1{}' - K_1K_3{}') & K_2K_1{}' - K_1K_2{}' \end{pmatrix} \end{aligned} \quad (2.56)$$

Here we denote λ^s and λ^a in Eqn.2.53 are the symmetric and antisymmetric factors to the spin orbit Hamiltonian, the parameter μ is an empirical parameter and α is the ratio of the nonmetallic contribution to the metallic contribution for $\vec{G} = \vec{G}' = 0$ (Walter, Cohen, Petroff, & Balkanski, 1970).

In Eqn.2.57 we show that B_{nl} s.t.

$$B_{nl} = C\int_0^\infty j_l(Kr)R_{nl}(r)r^2dr \quad (2.57)$$

Here in Eqn.2.57 the constant C is the normalization constant of the function B_{nl} s.t.

$$\sum_{K\to 0} K^{-1} B_{nl}(K) = 1 \tag{2.58}$$

Therefore, this normalization constant C can be written as follows,

$$C = 3\left[\int_0^{\infty} r R_{nl}(r) r^2 dr\right]^{-1} \tag{2.59}$$

Here the R_{nl} functions in Eqn.2.59 are named Hartree-FockSlater orbitals (Herman, Skillman, & Arents, 1964).

3. BAND STRUCTURE FOR BULK SOLIDS

3.1. Fitting Form Factors For a Famous Bulk Solid *GaAs*

In Empirical Pseudopotential Method, we can calculate energy bands profile and wave functions (eigenvalues and eigenvectors) of a solid with a good accuracy.

Now we will afford a brief review of the EPM to apply the *GaAs* bulk solid. Here we can note that this definition useful for all zincblende materials with the similar way. Especially, we will define a band calculation including the spin-orbit interaction.

To define the direct lattice of the *GaAs* solid we use the three primitive translation vectors s.t.

$$\begin{aligned} \vec{a}_1 &= \frac{a}{2}(0,1,1) \\ \vec{a}_2 &= \frac{a}{2}(1,0,1) \\ \vec{a}_3 &= \frac{a}{2}(1,1,0) \end{aligned} \tag{3.1}$$

Here we know that the lattice constant is $a = 5.653$ Å for GaAs bulk material.

Gallium (Ga) and Arsenic (As) atoms are the basis elements for each cell and they set-apart by a distance vector $\vec{\tau} = \frac{a}{8}(1,1,1)$. If we ignore the manybody effects, we can write the electron transfer in a periodic potential $V(\vec{r})$ s.t.

$$V(\vec{r}) = V(\vec{r} + \vec{T}) \tag{3.2}$$

Where the vector $\vec{T}$ is any translation vector in the lattice. Because of the translation invariance of the periodic potential $V(\vec{r})$, we can write the Fourier expansion of the potential in Eqn.3.2 w.r.t. the reciprocal lattice vectors s.t.

$$V(\vec{r}) = \sum_{\vec{G}} V_{\vec{G}} e^{i\vec{G}\vec{r}} \tag{3.3}$$

Here we know that the reciprocal lattice vectors $\vec{G}$ satisfy an equation s.t. $\vec{G} \cdot \vec{a} = (integer) \cdot 2\pi$. Also, we can write primitive vectors of the reciprocal lattice s.t.

$$\vec{G}_1 = 2\pi \frac{(\vec{a}_2 \times \vec{a}_3)}{\vec{a}_1(\vec{a}_2 \times \vec{a}_3)}$$

$$\vec{G}_2 = 2\pi \frac{(\vec{a}_3 \times \vec{a}_1)}{\vec{a}_1(\vec{a}_2 \times \vec{a}_3)} \qquad (3.4)$$
$$\vec{G}_3 = 2\pi \frac{(\vec{a}_1 \times \vec{a}_2)}{\vec{a}_1(\vec{a}_2 \times \vec{a}_3)}$$

If we calculate the exact values of these reciprocal lattice vectors for GaAs, we get,

$$\vec{G}_1 = \frac{2\pi}{a}(-1,1,1)$$
$$\vec{G}_2 = \frac{2\pi}{a}(1,-1,1) \qquad (3.5)$$
$$\vec{G}_3 = \frac{2\pi}{a}(1,1,-1)$$

We know that the electrons interaction of close to the ion cores have strong atomic potential, so they have nearly atomic wave functions. Nevertheless, between the cores the electron interactions are much weaker so we can take the potential nearly constant potential. And between the cores the corresponding wave functions of electrons are almost plane waves which are orthogonal to the core wave functions (Kittel, 1963) (Harrison, 1980). Therefore, we can take the smoother pseudowave function in a bulk solid with using Bloch's theorem s.t.

$$\psi_{\vec{k}}(\vec{r}) \quad = e^{i\vec{k}\vec{r}} \sum_{\vec{G}} u_{\vec{G}}(\vec{k}) e^{i\vec{G}\cdot\vec{r}} \qquad (3.6)$$

Here we denote that $\vec{k}$ by Bloch function's wave vector in to the pseudo wave function. If we write this pseudo wave function in Eqn.3.6 in to the pseudo-Schrodinger equation for a single valence electron in a bulk solid we can find an equation with reciprocal space form,

$$\left(\frac{\hbar^2}{2m}\left|\vec{k}+\vec{G}\right|^2 + V_0 - E(\vec{k})\right) u_{\vec{G}}(\vec{k}) + \sum_{\vec{G}} V_{\vec{G}-\vec{G}'} u_{\vec{G}'}(\vec{k}) = 0 \qquad (3.7)$$

To get electronic band profile of a bulk solid like GaAs we plot the eigenvalues E versus wave vector $\vec{k}$. In the Eqn.3.7 we use a constant potential V_0. This potential term is not important for a bulk solid but it is very important to set the band offsets for a heterostructure like superlattice.

Now we study on an eigenvalue eigenfunction problem with solving the Eqn.3.7. The dimension of the matrix which we use to solve eigenvalue problem depends on the number of $\vec{k}$ which we named wave vectors. We write our eigenvalue problem with using MATHEMATICA program. We take 100 terms wave vectors in our calculation on the directions Γ [000] to the X [100]. For more accurate solutions you can take the number of wave vectors much larger range. So, we study on a matrix with dimension of 100x100 and if we add the spin orbit interaction then we have 200x200 matrix.

Here we write only needed reciprocal lattice vectors $\vec{G}$ s.t.

$$\vec{G}_0 = \frac{2\pi}{a}(0,0,0)$$
$$\vec{G}_1 = \frac{2\pi}{a}(1,1,1)$$
$$\vec{G}_2 = \frac{2\pi}{a}(1,1,-1)$$
$$\vec{G}_3 = \frac{2\pi}{a}(1,-1,1)$$
$$\vec{G}_4 = \frac{2\pi}{a}(1,-1,-1)$$
$$\vec{G}_5 = \frac{2\pi}{a}(-1,1,1)$$
$$\vec{G}_6 = \frac{2\pi}{a}(-1,1,-1)$$
$$\vec{G}_7 = \frac{2\pi}{a}(-1,-1,1)$$
$$\vec{G}_8 = \frac{2\pi}{a}(-1,-1,-1)$$
$$\vec{G}_9 = \frac{2\pi}{a}(0,0,2)$$
$$\vec{G}_{10} = \frac{2\pi}{a}(0,0,-2)$$
$$\vec{G}_{11} = \frac{2\pi}{a}(0,2,0)$$
$$\vec{G}_{12} = \frac{2\pi}{a}(0,-2,0)$$
$$\vec{G}_{13} = \frac{2\pi}{a}(2,0,0) \qquad (3.8)$$

$$\vec{G}_{14} = \frac{2\pi}{a}(-2,0,0)$$

We note that the spin up and the spin down components of the spin couples the spin orbit interaction. The spin orbit matrix element in the pseudopotential theory contains $\vec{G}$ and $\vec{G}'$ w.r.t the wave vector $\vec{k}$ s.t.

$$V^{SO}_{\vec{G}-\vec{G}'} = \frac{i\hbar^2}{4m^2c^2}\Gamma\langle S|\vec{\sigma}|S'\rangle \cdot (\vec{G} - \vec{G}') \times (\vec{G}' + \vec{k})V_{\vec{G}-\vec{G}'} \tag{3.9}$$

In the Eqn.3.9 we denote the pseudopotential coefficients $V_{\vec{G}-\vec{G}'}$ which we write w.r.t the form factors. Also we write the spin orientation $|S\rangle$ and the Pauli spin matrices $\vec{\sigma}$ in Eqn.3.9. In the same equation Γ is a multiplicative factor Γ requires discussion.

In the face-centered cubic (FCC) the gallium arsenide (GaAs) bulk solid is basicly pictured s.t. the gallium and arsenic atoms on FCC lattice. Here we use as a bases which gives us the positions with distance vector $\vec{\tau} = \frac{a}{8}(1,1,1)$. In this procedure the lattice potential with pseudopotential coefficients can be written as,

$$V_{\vec{G}-\vec{G}'} = {V_{\vec{G}-\vec{G}'}}^{S} \cos\big((\vec{G} - \vec{G}') \cdot \vec{\tau}\big) - i{V_{\vec{G}-\vec{G}'}}^{A} \sin\big((\vec{G} - \vec{G}') \cdot \vec{\tau}\big) \tag{3.10}$$

Here we denote ${V_{\vec{G}-\vec{G}'}}^{S}$ is the symmetric pseudopotential form factors and ${V_{\vec{G}-\vec{G}'}}^{A}$ is the asymmetric pseudopotential form factors. In our calculation for GaAs band structure, we take the plane $z = 0$ is midway at the point Γ [000].

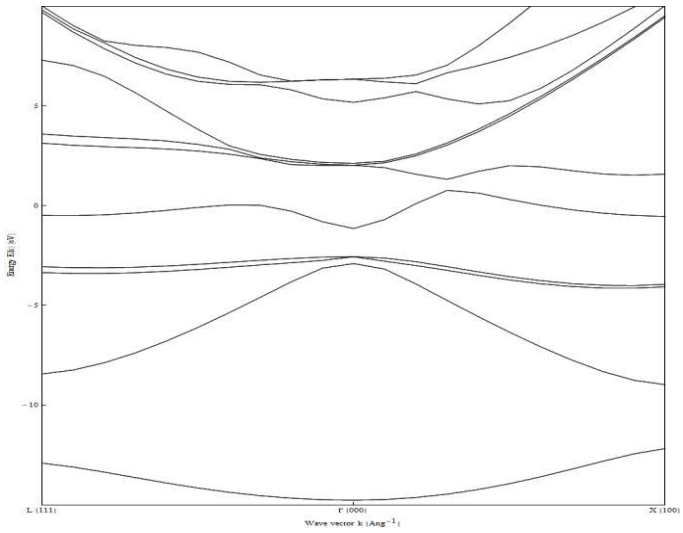

Figure 3.1. *Band diagram of GaAs with using Local EPM which including Spin Orbit interaction.*

To get the band structure of GaAs as shown in the Fig.3.1 we set up four 200x200 matrix form of Hamiltonian in Eqn.3.7 and Eqn.3.9 with including spin orbit interactions. Here we set the diagonals with spin orbit potential in Eqn.3.9 and the off-diagonals not include the spin orbit term. We calculate the eigenvalue problem with 200x200 matrix equation for each wave vector $\vec{k}$. This means that we set a do loop in the MATHEMATICA program for wave vector $\vec{k}$, 100 different positions. Here we get the energy E_n w.r.t $\vec{k}$ which is doubly degenerate values. We calculate the band structure of GaAs as in the Fig.3.1 for the different orientations of the wave vector $\vec{k}$. One of the directions start the Γ point to the X point ($[000]\ to\ [100]$) the other way start the Γ point to the L point ($[000]\ to\ [111]$).

Table 3.1. *GaAs Pseudopotential form factors at 300 K which we fitted in our own algorithm.*

Form Factors	Values
V_3^S	-0.27
V_4^S	0
V_8^S	0.02
V_{11}^S	0.07
V_3^A	0.091
V_4^A	0.001
V_8^A	0
V_{11}^A	0.01
Γ	3600
$\frac{m}{m_0}$	0.9

Table 3.1. shows the pseudopotential form factors and Γ constant. We use our algorithm on MATHEMATICA to find these parameters with fitting the experimental results of GaAs at 300K.

4. SUPERLATTICES EMPIRICAL PSEUDOPOTENTIAL METHOD (SEPM)

4.1. Theoretical Concept of SEPM

A new demonstration for the superlattice band modelling for the pseudopotential derived by Dante and Tilton. (Dente & Tilton, 1999).

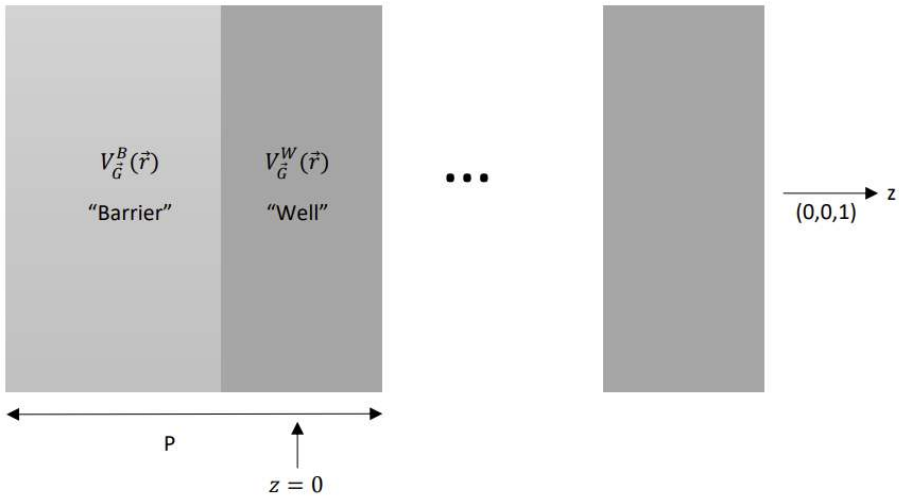

Figure 4.1. *Chemical formula of paracetamol*

In Fig.4.1 we consider a superlattice structure for two different materials. Here we denote P is the thickness of a barrier well pairs for the grown direction z ([001]). We also denote w as the thickness of the well layers and $(P - w)$ as the thickness of the barrier layers. The charge distributions in the interfaces may ignore when the well and barrier materials are lattice matched. If it is so, we can write the superlattice effective potential $V(\vec{r})$ with the sun over component pseudopotentials s.t.

$$V(\vec{r}) = rect(\frac{Z}{W}) \sum_{\vec{G}} V_{\vec{G}}^{W} e^{i\vec{G}\vec{r}} + \left[1 - rect(\frac{Z}{W})\right] \cdot \sum_{\vec{G}} V_{\vec{G}}^{B} e^{i\vec{G}\vec{r}} \qquad (4.1)$$

Here we denote $V_{\vec{G}}^{W}$ is the pseudopotential coefficients for Well materials and $V_{\vec{G}}^{B}$ is the pseudopotential coefficients for Barrier materials.

We also use the periodic rectangle function with using finite Fourier series formula s.t.

$$rect\left(\frac{z}{w}\right) = \sum_{n=-M}^{M} \frac{1}{n\pi} \sin\left(\frac{\pi w}{P} \cdot n\right) e^{i\left(\frac{2\pi n}{P}\right)\cdot z} \tag{4.2}$$

Here we limited M to allow the continuity between the different materials. If we increase the constant value M then the sharpness of the interface is increase, or vice versa.

In conclusion, the superlattice potential $V(\vec{r})$ is equal to the sum of two different parts, which the right-hand side term has two sum which one of that is over reciprocal vectors and the other is the superlattice wave vectors $\pm n\left(\frac{2\pi}{P}\right)$ s.t.

$$\begin{aligned} V(\vec{r}) = &\sum_{\vec{G}} \left[V_{\vec{G}}^{B} + \frac{W}{P}\left(V_{\vec{G}}^{W} - V_{\vec{G}}^{B}\right)\right] e^{i\vec{G}\vec{r}} \\ &+ \sum_{\vec{G}} \sum_{n\neq 0} \left(V_{\vec{G}}^{W} - V_{\vec{G}}^{B}\right) \frac{\sin\left(\frac{\pi W}{P} \cdot n\right)}{\pi n} e^{i\vec{G}\vec{r}} e^{i\left(\frac{2n\pi}{P}\right)\cdot z} \end{aligned} \tag{4.3}$$

Where the term $n = 0$ can be written as below as a limit position,

$$\lim_{n\to 0} \frac{\sin\left(\frac{\pi W}{P} \cdot n\right)}{\pi n} = \frac{w}{P} \tag{4.4}$$

We know that the $g = 0$ terms don't have any effects for bulk solids but this is so important for the superlattice structure. This $g = 0$ terms give us the band offsets between the materials in the superlattice structure.

Here we can write the well-known equation in quantum mechanics theory for a valance electron in the SL, which we know that, the effective Schrodinger equation s.t.

$$\left[-\frac{\hbar^2}{2m}\nabla^2 + V(\vec{r})\right]\psi = E\psi \tag{4.5}$$

The wave function of an electron in the superlattice structure can be written as below with using the plane wave expansion of the Bloch's functions s.t.

$$\psi(\vec{r}) = e^{i\vec{\xi}\vec{r}} \sum_{\vec{G}} \sum_{n=-N_F}^{N_F} \sum_{s} a_{\vec{G},n}^{s}(\vec{\xi}) e^{i\vec{G}\vec{r}} e^{i\left(\frac{2n\pi}{P}\right)\cdot z} |s\rangle \tag{4.6}$$

In Eqn.4.6 we denote $\vec{\xi}$ as a propagation wave vector of an electron in the SL structure, and we denote that $|s\rangle = |+\rangle$ is spin up and $|s\rangle = |+\rangle$ is spin-down. We denote

that $a^{+}_{\vec{G},n}$ and $a^{-}_{\vec{G},n}$ which define Bloch function coefficients for spin up and spin down respectively. The index n represent a constant value of superlattice space frequency. Here the limit positions of the index n in a range s.t. $-\frac{P}{a}+1 \leq n \leq \frac{P}{a}$.

If we use this Bloch function which we give in Eqn.4.6 in to the Eqn.4.5 then we have the effective Schrodinger equation like in Eqn.4.7. Here we take the second order derivative of the Bloch function and we use the inner product of functional theory. With using this eigenvalue problem, we get the eigenvalues $E(\vec{\xi})$ which are the energies and eigenvectors which are wave functions corresponding to the wave vectors of $\vec{\xi}$.

$$\frac{\hbar^2}{2m}\left[\left|\vec{G}_{\parallel}+\vec{\xi}_{\parallel}\right|^2+\left(G_z+\frac{2\pi n}{P}+\xi_z\right)^2\right]a^{s}_{\vec{G},n} + \sum_{\vec{G},n}\left\langle \vec{G}ns\middle|V\middle|\vec{G}'n's'\right\rangle a^{s}_{\vec{G},n} = E(\vec{\xi})a^{s}_{\vec{G},n} \tag{4.7}$$

The second term of left-hand side of Eqn.4.7 represents linear matrix form of the effective superlattice potential. In our MATHEMATICA program we solve the linear equation with matrix form of eigenvalue – eigenvector problem with include spin orbit interaction. We set a linear equation with matrix has DxD dimension s.t.

$$D = 200 \cdot \left(\frac{2P}{a}\right) \tag{4.8}$$

The matrix element of the second term of right-hand side of Eqn.4.7 can be written as follows;

$$\left\langle \vec{G}ns\middle|V(\vec{r})\middle|\vec{G}'n's'\right\rangle = V^{B}_{\vec{G}-\vec{G}'} + \frac{\sin\left(\frac{\pi w}{P}(n-n')\right)}{\pi(n-n')}\cdot\left(V^{W}_{\vec{G}-\vec{G}'}-V^{B}_{\vec{G}-\vec{G}'}\right) \tag{4.9}$$

In Eqn.4.9 we assume that $n \neq n'$, but if we take $n = n'$ which gives the diagonal blocks s.t.

$$\left\langle \vec{G}ns\middle|V(\vec{r})\middle|\vec{G}'n's'\right\rangle = V^{B}_{\vec{G}-\vec{G}'} + \frac{w}{P}\cdot\left(V^{W}_{\vec{G}-\vec{G}'}-V^{B}_{\vec{G}-\vec{G}'}\right) \tag{4.10}$$

In the diagonal we have the 200x200 blocks which represents like a bulk material approximation potential with each layer in the superlattice structure. Here we demonstrated a superlattice structure which has two components but as we said before

you can easily use this phenomenon for any number of components. Therefore, these pseudopotential calculations require six form factors and one Γ constant for each two components. In addition, we use one band-offset value in the calculation. We note that this number of parameters is an important point for superlattice band modelling. The number of parameters which we use in the calculation for two components superlattice is equal to the 8x8 $\vec{k} \cdot \vec{p}$ method. Furthermore, we can say the significant parts of the Superlattice Empirical Pseudopotential Method w.r.t $\vec{k} \cdot \vec{p}$ method s.t.

- We don't accept small momentum in our calculations.
- We don't use the Envelope function approximation here.
- Here we don't have any uncertainties for boundary conditions.
- In the results we have 200 bands for each material which we use with superlattice structure. We can write a markable note that this number is 8 for $\vec{k} \cdot \vec{p}$ mothod.

4.2. Verification For A Famous Superlattice *GaAs/AlGaAs*

We know that $GaAs/Al_xGa_{1-x}As$ superlattice structure is one of the most investigated superlattice in the literature. In recent times, the valence hh-lh band distributions of this superlattice structure were measured by using electrons recombination of acceptors. This result labelled by J. A. Kash *et al* as follows with Fig.4.2. (Kash, Zachau, Tischler, & Ekenberg, 1992);

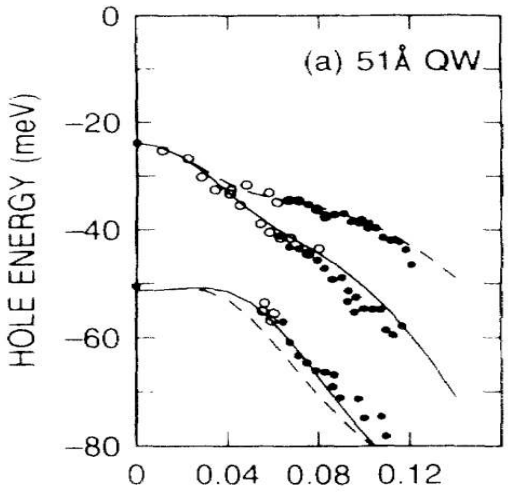

Figure 4.2. *Experimental data for a superlattice $GaAs/Al_{0.32}Ga_{0.68}As$ structure (Kash, Zachau, Tischler, & Ekenberg, 1992)*

Fig.4.2 shows experimental data from Ref. (Kash, Zachau, Tischler, & Ekenberg, 1992) for a 51 Å $GaAs$ as a well part of superlattice structure and the barrier part of the superlattice is 100 Å of $Al_{0.32}Ga_{0.68}As$.

For this well-known superlattice structure we use the Superlattice Empirical Pseudopotential Method which we describe in previous section. We also can compare the result with experimental data of $aAs/Al_{0.32}Ga_{0.68}As$ in the Fig.4.2.

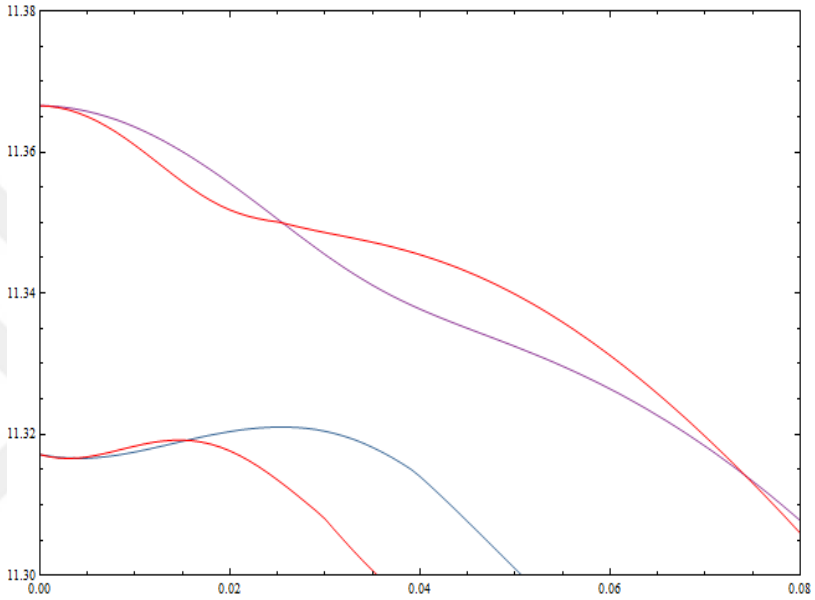

Figure 4.3. *Our results of valance subbands for the $GaAs/Al_{0.32}Ga_{0.68}$ superlattice with using SEPM which we modelling with MATHEMATICA. Red line curve for direction [110] and the other curves for [100] direction.*

In the Fig.4.3, we see that our results of valance subbands for the $GaAs/Al_{0.32}Ga_{0.68}$ superlattice with using SEPM which we modelling with MATHEMATICA. To get the results which we shown in Fig.4.3 first we use the bulk EPM calculation of *GaAs* and $Al_{0.32}Ga_{0.68}As$ to get the form factors which are the input parameters for the superlattice. We show these parameters in the Table 4.1. When we calculate these parameters, we fit the data from the ref. (Landolt-Bornstein, 1987). We use these parameters in Table 4.1 directly in the SEPM calculations with not any changes. In our calculations, we use band offset of $GaAs/Al_{0.32}Ga_{0.68}$ is 168meV (Kash, Zachau, Tischler, & Ekenberg, 1992). Which means that the valence band maximum of *GaAs* placed above the valance band maximum of $Al_{0.32}Ga_{0.68}$. In addition, we can note that, here we use the cutoff value N_F is equal 5 to get the result in Fig.4.3.

Table 4.1. *Pseudopotential form factors which fitting with MATHEMATICA for $Al_{0.32}Ga_{0.68}As$ and GaAs at 77K*

Form Factors	$GaAs$	$Al_{0.32}Ga_{0.68}As$
V_3^S	-0.235	-0.247
V_4^S	0	0
V_8^S	0	0.011
V_{11}^S	0.09	0.088
V_3^A	0.089	0.088
V_4^A	0	0.0337
V_8^A	0	0
V_{11}^A	0.0118	0.00982
Γ	3079	4100

5. TYPE II SUPERLATTICES (T2SL)

5.1. Type-II Superlattice Infrared Dedectors

For *InAs/GaSb* photodetectors which is one of the Type II superlattice (T2SL) is the most interest for development of detectors which named by Short – Mid – Long Wave Infrared s.t. SWIR - MWIP and LWIP. This Type-II superlattice infrared detector has many benefits for band gap engineering (Wei & Razeghi, 2004) and it suppress of Auger recombination (Grein, Young, & Ehrenreich, 1992) and this structure decrease the interband tunneling (Smith & Mailhiot, 1987).

In 2006 the $InAs/GaSb$ Type – II superlattice photodiode structure have been established (Rehm & Walther, 2006). We know this photodiode operating at the temperature 77K but it must operate at higher temperature and high quantum efficiencies. If we operate a superlattice structure at high temperature then we get low optical absorption and high dark current effects in the material. This is very important problem for this type superlattice and researchers try to solve this problem with using energy barriers. To compensate this, they dwell on barriers between bulk and superlattice structure.

There are many different types of superlattice structure for lattice match Type-II superlattices. Some of these are nBn design (Krishna, nBn structure based on InAs⁄GaSb type-II strained layer superlattices, 2007), PbIbN design (Krishna & Gautam, Performance improvement of longwave infrared photodetector based on type-II InAs/GaSb superlattices using unipolar current blocking layers, 2010), CBIRD structure (Ting, 2009), XBn design (Klipstein P. , 2011), “W” structure (Canedy, 2007) and “M” structure (Delaunay, 2009).

5.2. N Structure Superlattice

In the letter of our working group (Ergun & Aydinli, 2012), they introduce a new novel superlattice system which named as N structure. Under bias, this new structure augments the electron - hole overlap significantly. This N structure superlattice is like a pin diode. The N structure, which has opposite symmetry w.r.t M design. Here the $AlSb$ layer inserted between $InAs$ and $GaSb$ layers like an electron barrier. Overlap of the electron hole wavefunction increases on one side of the barrier part under the bias in a symmetrical barrier structure. But with the N structure we have asymmetrical barrier it

increases the absorption without any loss of overlap. Although the interface of $InAs$ and $AlSb$ materials is not lattice match perfectly, for N structure expected to reduce dark current significantly.

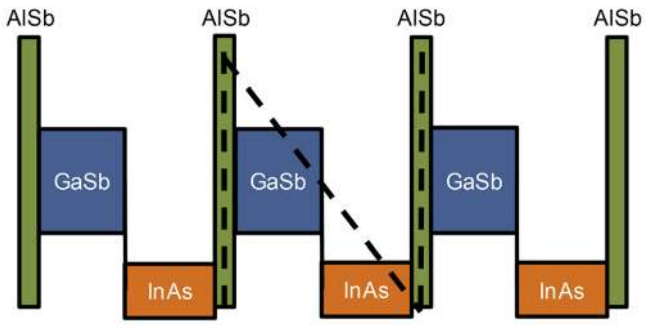

Figure 5.1. *Band profile of N structure with conduction and valance bands. (Ergun & Aydinli, 2012)*

In Fig.5.1 we show that the band profile structure of conduction and valance bands for N structure. As we have shown in Fig.5.1, name of the N structure is coming from the lineup of the successive materials which is like the capital letter N. In a standard pin diode structure, electron and hole wavefunctions shift in opposite directions under the bias. With inserting an $AlSb$ layer into the middle of the $GaSb$ layer cause to increase the overlap at the $InAs/GaSb$ interface. But, when we insert an $AlSb$ barrier between the $GaSb$ and $InAs$ layers, electron and hole wavefunctions are thrust off from the $AlSb$ interface and this increase the overlap at the $InAs/\ GaSb$ interface.

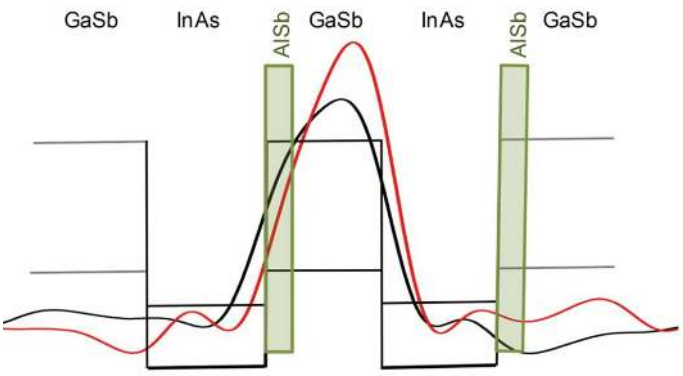

Figure 5.2. *The overlap wavefunction with (red line) and without (black line) AlSb barrier under 0.001 meV bias per period. These functions get with applying negative bias to the right side of the N structure. (Ergun & Aydinli, 2012)*

Fig.5.2. shows the overlap wavefunction with (red line) and without (black line) AlSb barrier under 0.001 meV bias per period. If the structure has no barrier (black line), the overlap integral of wavefunctions is shifted to the right-hand side of the $GaSb$ layer. But if we use the $AlSb$ barrier in the structure (red line) the overlap integral of wavefunctions is shifted to the $InAs/GaSb$ interface. Obviously, we can say that this $AlSb$ barrier increases the overlap at the $GaSb/InAs$ interface. Therefore, these calculations show that the absorption at the interface nearly %25 increases when we use the $AlSb$ barrier in the interface.

5.3. Band Structure Results of N Structure

With using empirical pseudopotential method (EPM) we obtained the interband transition energies of $InAs/GaSb$ structure and $InAs/AlSb/GaSb$ structure which we say N structure, based on T2SL. The aim of this thesis we investigate and compare the band structures and *hh-lh* splitting energies of $AlSb/GaSb$ structure with the variation of the $InAs$ layers (Akel, Hostut, Tansel, & Ergun, 2018).

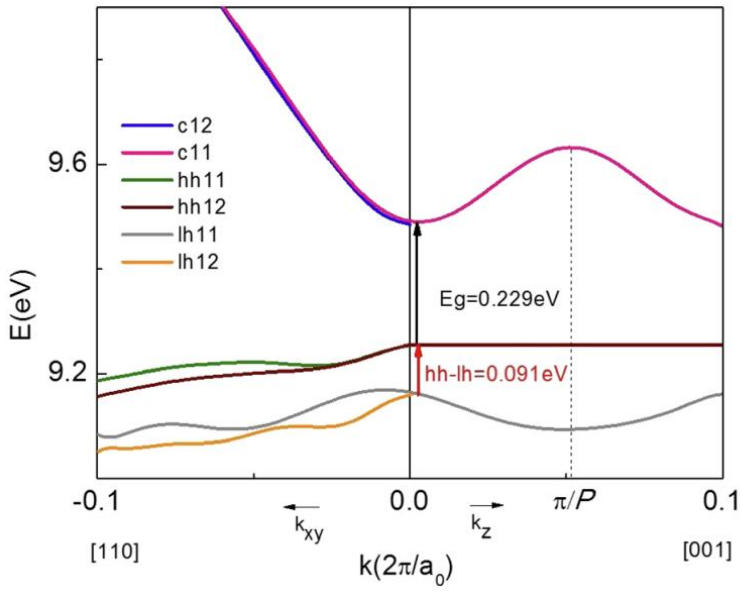

Figure 5.3. *The valance and conduction band-structure of InAs/GaSb structure with 10.5ML / 9ML T2SL. This is showing distribution of energy w.r.t. electron wavevector (k_{xy}) in plane and the electron wavevector (k_z) in the growth direction for MWIR T2SL. The vertical dashed line for [001] direction represents the conduction bands c11 and c12 zone edges at ($\frac{\pi}{P}$). Here P is define the periodical length of structure.*

Here the Fig.5.3 shows us the $E(k)$ distribution w.r.t. $\vec{k}$ vector of standard $InAs/GaSb$ T2SL. We get both directions, in-plane ($k_x, k_y, or\ k_\perp$) and parallel to the growth direction (k_z). The in-plane distribution along [110] direction is shown on the left-hand side of the Fig.5.3, although we show the distribution in the growth direction z on the right hand side of the Fig.5.3. In this structure of the superlattice we use the $InAs$ thickness as 10.5 ML and $GaSb$ thicknes as 9 ML. This SL structure gives us the 229 meV band gap energy which corresponds to 5.4 μm in wavelength within the MWIR. Also in this band profile of SL structure the *hh-lh* splitting energy is 91 meV.

With using same EPM calculations for the superlattice structure of $InAs/AlSb/GaSb$ which is N-structure T2SL we get the same bandgap structure to compare standard T2SL structure.

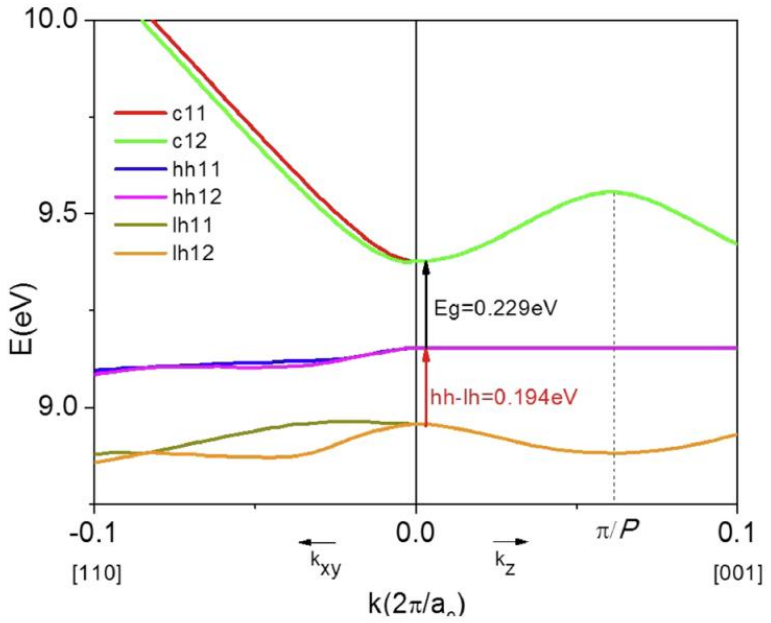

Figure 5.4. *The valance and conduction band-structure of InAs/AlSb/GaSb which is N structure with 7.5ML / 3ML / 6ML T2SL. This is showing distribution of energy w.r.t. electron wavevector (k_{xy}) in plane and the electron wavevector (k_z) in the growth direction for MWIR T2SL. The vertical dashed line for [001] direction represents the conduction bands c11 and c12 zone edges at ($\frac{\pi}{P}$). Here P is define the periodical length of structure.*

In the Fig.5.4. we show that the valance and conduction band-structure of $(InAs)_{7.5}/(AlSb)_3/(GaSb)_6$ which is N structure T2SL. This is showing distribution of energy w.r.t. electron wavevector (k_{xy}) in plane and the electron wavevector (k_z) in the

growth direction for MWIR T2SL. The important difference between the standard structure in Fig.5.3 and the N structure in Fig.5.4 is larger *hh-lh* splitting energy as we derive in our calculation s.t. 194 *meV*. Then now, we calculate the bandgap results and *hh-lh* splitting energy data as a function of the $AlSb$ layer thickness in the N type superlattice structure.

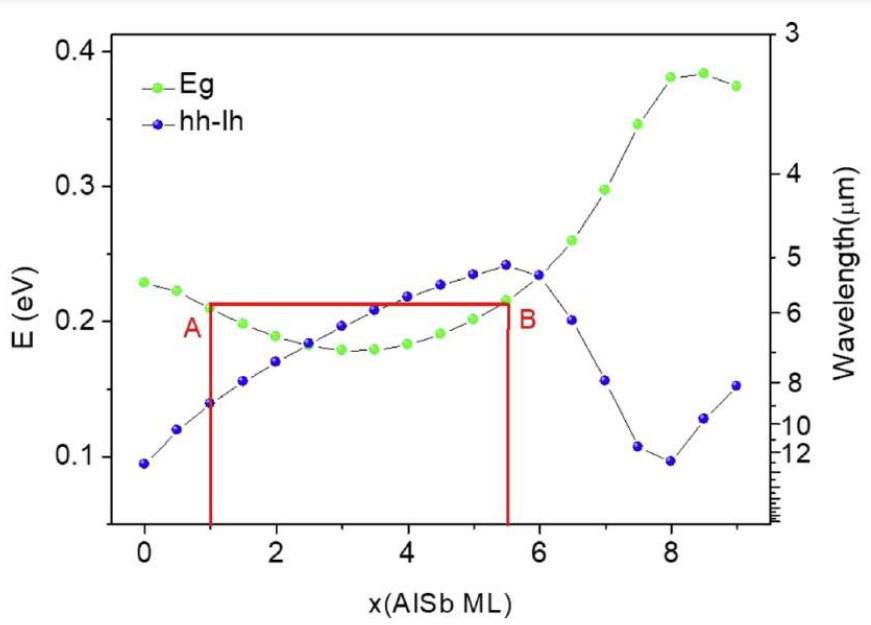

Figure 5.5. *Deviation of the bandgap and hh-lh splitting energies w.r.t. the AlSb monolayers in the interface* $(InAs)_{10.5}/(AlSb)_x/(GaSb)_{9-x}$ *structure. The green dashed line is deviation of the bandgap energy and the blue dashed line is deviation of the hh-lh splitting energy.*

In the Fig.5.5 we show the deviation of the bandgap and hh-lh splitting energies w.r.t. the AlSb monolayers in the interface $(InAs)_{10.5}/(AlSb)_x/(GaSb)_{9-x}$ structure. As we have shown in the Fig.5.5 if the $AlSb$ layer thickness increases then we see that the hh-lh splitting energy increases with 90 *meV* to 242 *meV*. But if we increase the AlSb ML's more than the 5 ML, then it decreases back to 90 *meV*. Vice versa, in the Fig.5.5 we see that if the $AlSb$ layer thickness increases then we see that the bandgap energy decreases with 229 *meV* (5.4 μm) to 178 *meV* (7 μm). But if we increase the AlSb ML's more than the 4 ML, then it increases quickly up to 384 meV (3.22 μm). Also, again in the Fig.5.5 we use the letters A and B label which gives us the same bandgap value 207 *meV* with the thicknesses of 1ML and 3.5ML. On the other hand we get the *hh-lh* splitting energy for the corner we labeled A and B are 138 *meV* and 242 *meV* are respectively.

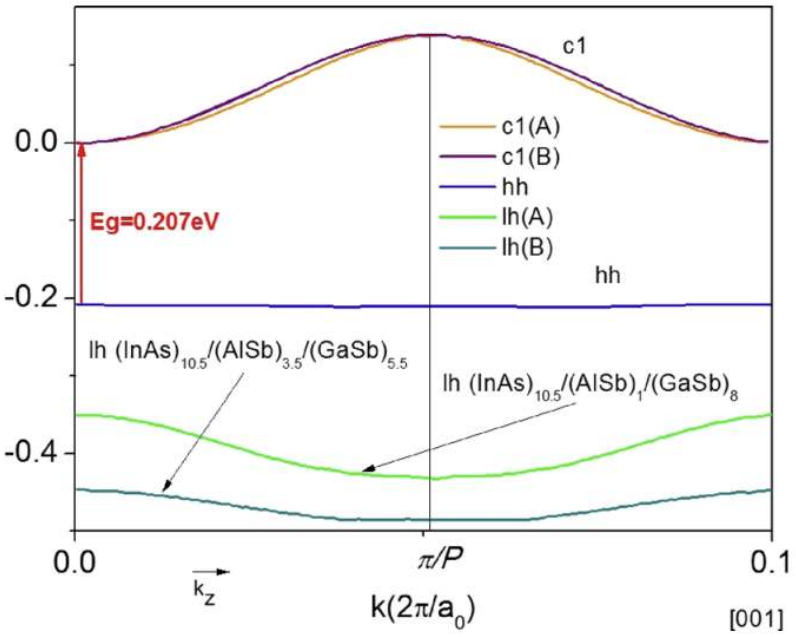

Figure 5.6. *The conduction and valance band energy comparison for* $(InAs)_{10.5}/(AlSb)_{3.5}/(GaSb)_{5.5}$ $(blue\ line)$ *and* $(InAs)_{10.5}/(AlSb)_{1}/(GaSb)_{8}$ *(green line) structures in the growth direction* (k_z).

According to our calculations the energy function $E(k)$ distribution w.r.t. wave vector $\vec{k}$ for both $(InAs)_{10.5}/(AlSb)_{3.5}/(GaSb)_{5.5}$ (blue line) and $(InAs)_{10.5}/(AlSb)_{1}/(GaSb)_{8}$ (green line) structures which their $c1$-$hh1$ bands overlapped each other. But the light hole deviations are not as shown in Fig.5.6. The effective masses of electrons and light hole, which we obtained from our calculations for different type of SL structure are listed as below Table 5.1.

Table 5.1. *The effective masses of electrons and light hole which we obtained from our calculations for different type of SL structure.*

	$m_e[001]$	$m_e[110]$	$m_{lh}[001]$	$m_{lh}[110]$
$(InAs)_{10.5}/(GaSb)_{9}$	0.028	0.0142	0.035	0.074
$(InAs)_{10.5}/(AlSb)_{1}/(GaSb)_{8}$	0.0308	0.0152	0.0385	0.0734
$(InAs)_{10.5}/(AlSb)_{5.5}/(GaSb)_{3.5}$	0.0396	0.01638	0.0901	…
$(InAs)_{7.5}/(AlSb)_{3}/(GaSb)_{6}$	0.0363	0.01656	0.05953	0.1076
$(InAs)_{17}/(AlSb)_{3}/(GaSb)_{6}$	0.0333	0.01371	0.0562	0.1307

There is no important increase with in the effective masses on the both directions in plane or vertical w.r.t the increasing of the $AlSb$ thickness in the N type superlattice structure. Hence, this situation shows us deviation of the thickness has no effect for the electron diffusion length and device performance of the superlattice structure. We know that it is very important for the detectors, the higher *hh-lh* splitting energy is so significant for suppressing the electron-hole recombination to Auger recombination (Tidrow, Zheng, & Barcikowski, 2009).

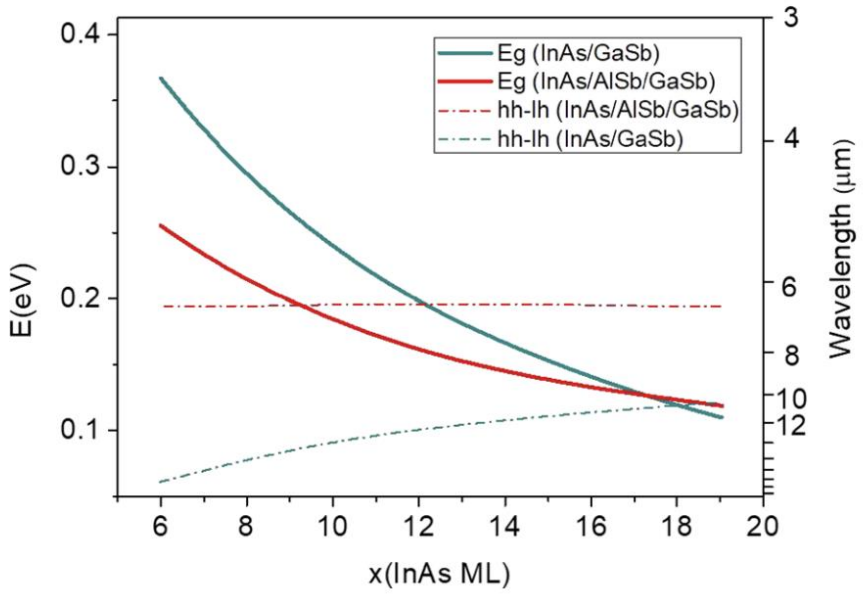

Figure 5.7. *The energy gap and hh-lh splitting energies w.r.t. the deviation of the InAs ML in the structure of* $(InAs)_x/\ (AlSb)_3/(GaSb)_6$ *T2SL. Here x is differed from 6 to 19 ML.*

Also, our calculations includes mid- and long wavelength performances of $InAs/AlSb/GaSb$ and standard $InAs/GaSb$ T2SL structures depend on the thickness of the $InAs$ layers. Here we use two different types of superlattice structure s.t. $(InAs)_x/\ (AlSb)_3/(GaSb)_6$ structure and $(InAs)_x/(GaSb)_9$ structure. For these two superlattice structures we change the variable x from 6ML to the 19ML. We show how the bandgap end the hh-lh splitting energy differ in the Fig.5.7 w.r.t. different type of the superlattice. For both SL structures the bandgap energies increasing w.r.t. thickness of the $InAs$ layers. We calculated the E_g values of 354 meV for $(InAs)_6/(GaSb)_9$ SL and 248 meV (5 μm) for $(InAs)_6/\ (AlSb)_3/(GaSb)_6$ T2SL for 6ML of $InAs$ thickness. So, this means that both are within the MWIR. If we increase the $InAs$ thickness to the 17

ML, the Eg values of SL structures take account 124 *meV* which is in the long wavelength range (LWIR). One of the important results in our calculations is in the Fig.5.7. s.t. when we increase the *InAs* ML in the superlattice structure the band gap energy decrease below the *hh-lh* split of gap. The important thing of this result is the difference between band gap energy and *hh-lh* change from MWIR to LWIR so this means that the band gap energy is less than the *hh-lh* splitting energy.

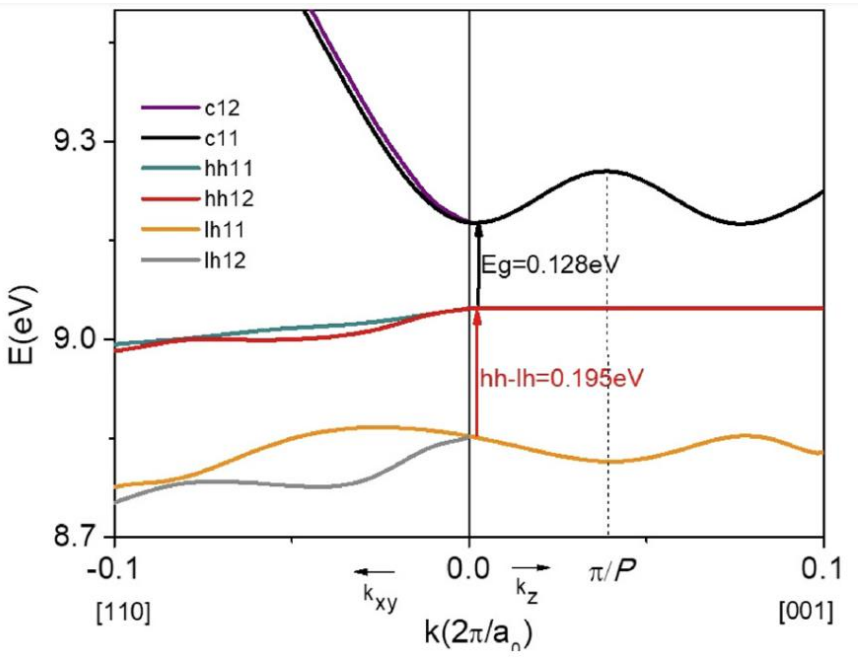

Figure 5.8. *The valance and conduction band-structure of InAs/AlSb/GaSb which is N structure with 17ML / 3ML / 6ML T2SL. This is showing distribution of energy w.r.t. electron wavevector (k_{xy}) in plane and the electron wavevector (k_z) in the growth direction for MWIR T2SL. The vertical dashed line for [001] direction represents the conduction bands c11 and c12 zone edges at ($\frac{\pi}{P}$). Here P is define the periodical length of structure.*

In the graph as we shown with Fig.5.8 gives the valance and conduction band-structure of InAs/AlSb/GaSb which is N structure with 17ML / 3ML / 6ML T2SL. This superlattice structure have the band gap 128 *meV* which means that have wavelength of 9.7 μm. Also, this structure have the hh-lh splitting energy 195 *meV* the band-structure and energy dispersion relation for 17 ML $InAs$, 3 ML $AlSb$, and 6 ML $GaSb$ T2SL structure with 128 *meV* bandgap energy. This corresponds to 9.7 μm in wavelength. In Fig.5.8, *hh-lh* splitting energy appears to be 195 *meV*. Again, we can note that the splitting energy is larger than the bandgap. Consequently, this superlattice structure provide to decrease of Auger recombination for a long wavelength superlattice design such as

$InAs/AlSb/GaSb$ structure. As a result, the $InAs/AlSb/GaSb$ superlattice structure demonstrations a hopeful manner to operate the material at higher temperatures.

6. CONCLUSIONS

In this thesis first of all we have demonstrated the theoretical formulation of Hamiltonian equation of a superlattice with using Superlattice Empirical Pseudopotential Method (SEPM). Then we investigate the band structure of the novel type-II superlattice N-Structure w.r.t. different MLs. We write our own modelling program to solve Hamiltonian equation, which we get in the matrix form in Appendix. We use the Mathematica program to solve the Eigenvalues and Eigenvectors that gives the electronics data of N-Structure.

As a result, we have established the application superlattice pseudopotential method for $InAs/GaSb$ and $InAs/AlSb/GaSb$ T2SLs detector structures with deviation of the thickness of the *AlSb* layers, operating from MWIR to LWIR. Our superlattice pseudopotential method calculations, which gives us the band structure, demonstration that increasing of the $AlSb$ thickness within the N structure caused increase in *hh-lh* splitting energy for the $(InAs)_{10.5}/\ (AlSb)_x/(GaSb)_{9-x}$ T2SL structure. Furthermore, as an important result for the $(InAs)_x/\ (AlSb)_3/(GaSb)_6$ SL structure is *hh-lh* splitting energy is 195 meV , which gives us a detector design operating with higher temperature in LWIR region.

REFERENCES

Akel, K., Hostut, M., Tansel, T., & Ergun, Y. (2018). Large hh-lh splitting energy for InAs/AlSb/GaSb based N-structure photodetectors. *JOURNAL OF APPLIED PHYSICS,123*, 025703.

Bester, G. (2009). Electronic excitations in nanostructures: an empirical pseudopotential based approach. *Journal of Physics: Condensed Matter*, 023202.

Bloom, S., & Bergstresser, T. (1968). Band structure of α-Sn, InSb and CdTe including spin-orbit effects. *Solid State Communications*, 465-467.

Böer, K. W., & Pohl, U. W. (2017). Quantum mechanics of electrons in crystals. *Semiconductor Physics*, 1-36.

C. L. Canedy, E. H. (2007). Antimonide Type-II "W" Photodiodes with Long-Wave Infrared R 0 A Comparable to HgCdTe. *J. Electron. Mater*, 852-856.

Canedy, C. L. (2007). Antimonide Type-II "W" Photodiodes with Long-Wave Infrared RoA Comparable to HgCdTe. *J. Electron. Mater.*, 852 - 856.

Chelikowsky, J., & Cohen, M. (1974). Electronic structure of silicon. *Physical Review B*, 153-158.

Cohen, M. L. (1979). Momentum-space formalism for the total energy of solids. *J. Phys. C: Solid State Phys.*, 4409.

Cohen, M. L. (2011). Nanotubes, nanoscience, and nanotechnology. *Materials Science and Engineering: C 15*, 1-11.

Cohen, M. L., & Chelikowsky, J. R. (1988). *Electronic Structure and Optical Properties of Semiconductors.* Berlin: Springer-Verlag.

David Z.-Y. Ting, C. J. (2009). A high-performance long wavelength superlattice complementary barrier infrared detector. *Appl. Phys. Lett.* , 023508.

Delaunay, P. Y. (2009). Background Limited Performance of Long Wavelength Infrared Focal Plane Arrays Fabricated From M-Structure InAs–GaSb Superlattices. *IEEE J. Quantum Electronics*, 157 - 162.

Dente, G. C., & Tilton, M. L. (1999). Pseudopotential methods for superlattices: Applications to mid-infrared semiconductor lasers. *J. Appl. Phys.*, 1420.

Ergun, Y., & Aydinli, A. (2012). "N" structure for type-II superlattice photodetectors. *APPLIED PHYSICS LETTERS*, 073505.

Fermi, E. (1934). Sopra lo spostamento per pressione delle righe elevate delle serie spettrali. *Il Nuovo Cimento*, 157-166.

Grein, C. H., Young, P. M., & Ehrenreich, H. (1992). Minority carrier lifetimes in ideal InGaSb/InAs superlattices. *Applied Physics Letters*, 2905 - 2907.

Harrison, W. A. (1980). *Electronic Structure and the Properties of Solids.* San Francisco: W. H. Freeman.

Hellmann, H. (1935). A new approximation method in the problem of many electrons. *J. Chem. Phys.*, 61.

Herman, F., Skillman, S., & Arents, J. (1964). Atomic Structure Calculations. *Journal of The Electrochemical Society*, 87C.

J. B. Rodriguez, E. P. (2007). nBn Structure Based on InAs/GaSb Type-II Strained Layer Superlattices. *Applied Physics Letters*, 043514.

J.R., C., & M.L., C. (1976). Nonlocal pseudopotential calculations for the electronic structure of eleven diamond and zinc-blende semiconductors. *Physical Review B*, 556-582.

Kash, J. A., Zachau, M., Tischler, M. A., & Ekenberg, U. (1992). Anisotropic Valence Bands in Quantum Wells: Quantitative Comparison of Theory and Experiment. *Phys. Rev. Lett.*, 2260.

Kittel, C. (1963). *Quantum Theory of Solids.* New York: Wiley.

Klipstein, P. (2011). XBn barrier photodetectors based on InAsSb with high operating temperatures. *Opt. Eng.*, 061002.

Klipstein, P. C. (2013). A k.p model of InAs/GaSb type II superlattice infrare. *" Infrared Phys. Technol.*, 53 – 59.

Krishna, S. (2007). nBn structure based on InAs/GaSb type-II strained layer superlattices. *Appl. Phys. Lett.*, 043514.

Krishna, S., & Gautam, N. (2010). Performance improvement of longwave infrared photodetector based on type-II InAs/GaSb superlattices using unipolar current blocking layers. *Appl. Phys. Lett.*, 231107.

Landolt-Bornstein. (1987). *Numerical Data and Functional Relationships in Science and Technology.* Berlin: Springer.

Liboff, R. (2003). *Introductory quantum mechanics.* MA: Addison-Wesley Reading.

N. Gautam, H. S. (2010). Performance improvement of longwave infrared photodetector based on type-II InAs/GaSb superlattices using unipolar current blocking layers. *Appl. Phys. Lett.* , 231107.

Omer Salihoglu, A. M. (2012). "N" structure for type-II superlattice photodetectors. *Appl. Phys. Lett.*, 073505.

P. Y. Delaunay, B. M. (2009). Background Limited Performance of Long Wavelength Infrared Focal Plane Arrays Fabricated From M-Structure InAs–GaSb Superlattices. *IEEE Journal of Quantum Electronics*, 157-162.

Phillips, J., & Kleinman, L. (1959). New method for calculating wave functions in crystals and molecules. *Physical Review*, 287-294.

Razeghi, M., & Pour, S. A. (2012). Revolutionary development of Type-II GaSb/InAs superlatices for third generation of IR imaging. *Proc. SPIE*, 835310.

Rehm, R., & Walther, M. e. (2006). Dual-colour thermal imaging with InAs/GaSb superlattices in mid-wavelength infrared spectral range. *Electron. Lett.*, 577 - 578.

Saravia, L., & Brust, D. (1968). Spin Splitting and the Ultraviolet Absorption of Ge. . *Physical Review*, 915-923.

Smith, D. L., & Mailhiot, C. (1987). Proposal for strained type II superlattice infrared detectors. *J. Appl. Phys*, 2545 - 2548.

Tidrow, M. Z., Zheng, L., & Barcikowski, H. (2009). Recent succes on SLS FPAs and PDA's new direction for development. *Proc. SPIE*, 72981O.

Ting, D. Z. (2009). Appl. Phys. Lett. *A high-performance long wavelength superlattice complementary barrier infrared detector*, 023508.

U. Kaya, M. H. (2013). Theoretical investigation of InAs/GaSb type-II pin superlattice infrared detector in the mid wavelength infrared range. *Journal of Applied Physics* , 083717.

Walter, J. P., Cohen, M. L., Petroff, Y., & Balkanski, M. (1970). Calculated and Measured Reflectivity of ZnTe and ZnSe. *Physical Review B*, 2661-2667.

Wei, Y. J., & Razeghi, M. (2004). Modeling of type-II InAsÕGaSb superlattices using an empirical tight-binding method and interface engineering. *PHYSICAL REVIEW B*, 085316.

Weisz, G. (1966). Band structure and Fermi surface of white tin. *Physical Review*, 504-518.

APPENDIX

With using Superlattice Empirical Pseudopotential Method (SEPM) we wrote the electronic band modelling algorithm in MATHEMATİCA program. In the program, the Hamiltonian matrix is represented as follows:

$$\langle S|H|S\rangle = \begin{bmatrix} H_{11} & H_{12} \\ H_{21} & H_{22} \end{bmatrix} = \begin{bmatrix} \langle S_1|H|S_1\rangle & \langle S_2|H|S_1\rangle \\ \langle S_1|H|S_2\rangle & \langle S_2|H|S_2\rangle \end{bmatrix} \tag{A-1}$$

H_{11} and H_{22} are for the spin up $S_1 = \begin{bmatrix} 1 \\ 0 \end{bmatrix}$ and spin down $S_2 = \begin{bmatrix} 0 \\ 1 \end{bmatrix}$; respectively. If we write the Pauli spin matrix

$$\vec{\sigma} = \sigma_x \hat{\imath} + \sigma_y \hat{\jmath} + \sigma_z \hat{k} \tag{A-2}$$

in the vector form, H_{11} and H_{22} including spin-orbit hamiltonian H_{SO} , superlattice potential V_{SL} and also kinetic term H_{kin} are given by

$$H = H_{SO} + V_{SL} + H_{kin} \tag{A-3}$$

Non-diagonal terms do not include potential and kinetic terms, where spin H_{SO} term is given as follows for H_{11}:

$$H_{SO}(i,j,n,n') =$$

$$\frac{i\hbar^2}{4{m_0}^2c^2}\langle S_1|\vec{\sigma}|S_1\rangle\left[\vec{G}_i - \vec{G}_j\right]\otimes\left[\vec{G}_j + \vec{\xi} + \frac{2\pi n}{P}\hat{k}\right]\sum_{l=1}^{N}\frac{w_l}{P}\cdot\Gamma_l V_l\left[\vec{G}_i - \vec{G}_j\right] \tag{A-4}$$

In Eqn.*A-4* we derive $H_{SO}(i,j,n,n')$ for $n = n'$ and $\vec{G}_i - \vec{G}_j \neq 0$ while $\vec{G}_i \neq 0$ or $\vec{G}_j \neq 0$.

$$H_{SO}(i,j,n,n') =$$

$$\frac{i\hbar^2}{4{m_0}^2c^2}\langle S_1|\vec{\sigma}|S_1\rangle\left[\vec{G}_i - \vec{G}_j + \frac{2\pi(n-n')}{P}\hat{k}\right]\otimes\left[\vec{G}_j + \vec{\xi}\right.$$

$$\left. + \frac{2\pi n'}{P}\hat{k}\right]\sum_{l=1}^{N}\left(\frac{\sin\left(\frac{\pi w_l}{P}(n-n')\right)}{\pi(n-n')}\right)e^{-i\left(\frac{2\pi(n-n')}{P}\left(\frac{w_l}{2}+\sum_{m\geq 1}^{l-1}w_m\right)\right)} \tag{A-5}$$

$$\cdot\,\Gamma_l V_l\left[\vec{G}_i - \vec{G}_j\right]$$

In Eqn.*A-5* we derive $H_{SO}(i,j,n,n')$ for $n \neq n'$ and $\vec{G}_i - \vec{G}_j \neq 0$ while $\vec{G}_i \neq 0$ or $\vec{G}_j \neq 0$.

Other matrix terms are easily obtained by changing the spin matrix (S1, S2)

$$V_{SL}{}^{11}(i,j,n,n') = \sum_{l=1}^{N} \frac{w_l}{P} \cdot V_l\left[\vec{G}_i - \vec{G}_j\right] \tag{A-6}$$

In Eqn.*A-6* we derive $V_{SL}{}^{11}(i,j,n,n')$ for $n = n'$ and $\vec{G}_i - \vec{G}_j \neq 0$ while $\vec{G}_i \neq 0$ or $\vec{G}_j \neq 0$.

$$V_{SL}{}^{11}(i,j,n,n') = \sum_{l=1}^{N} \left(\frac{\sin\left(\frac{\pi w_l}{P}(n-n')\right)}{\pi(n-n')} \right) e^{-i\left(\frac{2\pi(n-n')}{P}\left(\frac{w_l}{2}+\sum_{m\geq 1}^{l-1} w_m\right)\right)} \cdot V_l\left[\vec{G}_i - \vec{G}_j\right] \tag{A-7}$$

In Eqn.*A-7* we derive $V_{SL}{}^{11}(i,j,n,n')$ for $n \neq n'$ and $\vec{G}_i - \vec{G}_j \neq 0$ while $\vec{G}_i \neq 0$ or $\vec{G}_j \neq 0$.

Here also we note that;

$$V_{SL}{}^{11}(i,j,n,n') = V_{SL}{}^{22}(i,j,n,n') \tag{A-8}$$

Finally, the kinetic term is:

$$E(\vec{\xi})_{SL}{}^{11}(i,j,n,n') = \left[\vec{G}_i + \vec{\xi} + \frac{2\pi n}{P}\hat{k}\right]^2 \tag{A-9}$$

In Eqn.*A-9* we derive $E(\vec{\xi})_{SL}{}^{11}(i,j,n,n')$ for $n = n'$ while $\vec{G}_i = \vec{G}_j$.

As the potential and kinetic terms are also satisfied as $E(\vec{\xi})_{SL}{}^{11}(i,j,n,n') = E(\vec{\xi})_{SL}{}^{22}(i,j,n,n')$ where N is the multilayer number [3 constituents ($InAs - AlSb - GaSb$) in this work], P is the total width of a period of SL, and n and n' are given as Eqn.88. $V_l\left[\vec{G}_i - \vec{G}_j\right]$ is the atomic form factor for l^{th} layer of SL.

CURRICULUM VITAE

ORCID ID: Please fill

Name Surname **: Kazim AKEL**

Foreign Language **: English**

Place and Year of Birth **:**

Email **:**

Education and Professional Background:

- 2006-2010, Dokuz Eylül University, Faculty of Art and Science, Mathematics Department

Publications and/or Scientific/Artistic Activities:

- 2017, Poster, *Band profile investigation for InAs/GaSb and InAs/AlSb/GaSb structure using SL Empirical Pseudopotential Method*, 9TH INTERNATIONAL CONFERENCE ON NANOMATERIALS, Tehran - IRAN
- 2017, Poster, *Band profile investigation for InAs/GaSb and InAs/AlSb/GaSb structure using SL Empirical Pseudopotential Method*, ÇUKUROVA UNIVERSITYINTERNATIONAL CONFERENCE ON CONDENSED MATTER AND MATERIALSSCIENCE , Adana – TURKEY
- 2018, Poster, *Wave Function Characteristics obtained by atomistic approach for superlattice photo dedectors in the SWIR,* BIT'xxs 8th Annual Congress ofNano Science and Technology / Postdam – GERMANY
- Akel, K., Hostut, M., Tansel, T., & Ergun, Y. (2018). Large hh-lh splitting energy for InAs/AlSb/GaSb based N-structure photodetectors. *JOURNAL OF APPLIED PHYSICS,123*, 025703.
- Akel, K., Hostut, M., Akın, T., & Ergun, Y. (2021). Interband optical absorption obtained by pseudopotential method for type-II InAs/GaSb SL photodetectors. JOURNAL OF PHYSICS D: APPLIED

Awards:

- 2014, PhD, National PhD Scholarship Program in the Priority Fields in Science and Technology , Tübitak - TURKEY.